A dynamical interpretation of the intensification of the winter North Atlantic jet stream in reanalysis

Alejandro Hermoso, Gwendal Rivière, Ben Harvey, John Methven, Sebastian Schemm

A dynamical interpretation of the intensification of the winter North Atlantic jet stream in reanalysis

Alejandro Hermoso,[a] Gwendal Rivière,[b] Ben Harvey,[c d] John Methven,[c] and Sebastian Schemm,[a]

[a] *Institute for Atmospheric and Climate Science, ETH Zurich, Zurich, Switzerland*

[b] *LMD/IPSL, École Normale Supérieure, PSL Research University, Sorbonne Université, École Polytechnique, CNRS, Paris, France*

[c] *Department of Meteorology, University of Reading, Reading, UK*

[d] *National Centre for Atmospheric Science, University of Reading, Reading, UK*

Corresponding author: Alejandro Hermoso, alejandro.hermoso@env.ethz.ch

ABSTRACT: Jet streams play an important role in determining weather variability and extremes. A better understanding of the mechanisms driving long-term changes in the jet is essential to successfully anticipate extreme meteorological events. This study analyzes the intensification trend of the North Atlantic jet using the ERA5 reanalysis and investigates the dynamical mechanisms involved. The results highlight the importance of an increase in diabatic heating in the free troposphere below the jet entrance over the Gulf Stream sector. This change in diabatic heating modifies the jet directly and produces a local intensification and a slight poleward shift. A two-dimensional frontal-geostrophic model illustrates this mechanism by considering the enhanced diabatic heating associated with the baroclinic growth of extratropical cyclones. The change in diabatic heating also affects the jet indirectly by increasing the mean baroclinicity and subsequent eddy momentum flux convergence. This indirect mechanism has also an effect downstream, where there is an acceleration of the jet core and reduced westerlies along the flanks, reducing the width of the jet. An idealized warming experiment confirms this mechanism by determining the jet response downstream of an idealized land-sea contrast. Finally, using a single-model ensemble of fully-coupled climate simulations, we show that the differences in the evolution of the North Atlantic jet are related to the latitude of the increase in baroclinicity, which has a large spread. What emerges from the model hierarchy is a consistent dynamical chain of mechanisms associated with the intensification trend of the North Atlantic jet stream.

1. Introduction

The processes that determine the position and intensity of jet streams, which drive daily weather variability and contribute to the development of extreme weather events, are an ongoing area of research (Shaw et al. 2016), particularly with regard to open questions about the future evolution of the North Atlantic jet (Woollings et al. 2012). The high degree of uncertainty regarding the future intensity and position of the North Atlantic jet translates directly into a high degree of uncertainty with regard to weather variability. For example, there is not yet a significant consensus on the sign of the projected annual precipitation change for 1.5° C and 2.0° C of warming (e.g., Fig. 4.32 in Chapter 4 of the IPCC AR6 (Lee et al. 2021)), which is likely attributable to a low signal to noise ratio. In particular, over the North Atlantic, Central, and Northern Europe, the sign of the annual precipitation changes remains, in contrast to the Mediterranean region, inconclusive because of a large inter-model spread (e.g., Fig. 4.42 e and Fig. 4.42 f in Chapter 4 of the IPCC AR6 (Lee et al. 2021)).

Baroclinicity measures the baroclinic growth potential of transient eddies (Charney 1947; Eady 1949). It is proportional to the horizontal temperature gradient - and by virtue of thermal wind balance thus to the vertical wind shear - and inversely proportional to the vertical temperature gradient, which is a measure of atmospheric stability (Lindzen and Farrell 1980). Baroclinic growth of transient eddies in turn maintains deep westerly tropospheric jets against surface friction through associated eddy momentum flux convergence (Hoskins et al. 1983; Vallis 2017). Due to this inherent link between mean baroclinicity, baroclinic growth, and eddy momentum flux convergence, the analysis of the life cycle of eddy-driven jets alongside baroclinicity and its forcing processes (e.g. latent heat release) becomes crucial for understanding regional climate changes in areas affected by storm tracks. Ambaum and Novak (2014) proposed a nonlinear oscillator model to describe the joint evolution of diabatic heating, mean baroclinicity and baroclinic growth. The proposed life cycle displays qualitative agreement to observations with peaks of intense heat flux indicative for intense storm activity that acts to reduce the mean baroclinicity. When baroclinicity becomes too low to maintain the baroclinic eddy generation, storm activity is reduced and baroclinicity is replenished by diabatic heating influenced for instance by the orography or a land-sea contrast (Brayshaw et al. 2011), allowing the cycle to be repeated. Increased diabatic heat release (e.g. as expected in a warmer atmosphere) and/or modified temperature gradients (e.g. as

expected at low levels due to Arctic amplification and at upper levels due to tropical warming) thus could both influence the life cycle of the storm track by changing the mean baroclinicity, which would also affect the jet via eddy momentum feedback.

In the Northern Hemisphere, two competing trends due to anthropogenic climate change act on the equator-to-pole temperature gradient. Near the surface, the meridional temperature gradient is decreased due to amplified polar warming, a phenomenon known as the Arctic Amplification (AA) (Screen and Simmonds 2010). In contrast, in the upper troposphere tropical warming increases the meridional temperature gradient and reduces tropospheric stability. This larger temperature increase in the tropics is produced because the atmosphere follows a moist adiabatic lapse rate (Held 1993). In a warmer climate, the amount of water vapor in the atmosphere is higher and consequently there is more latent heat release, which reduces the lapse rate, since the adiabatic cooling resulting from the ascent is partially offset by higher latent heating. Jet streams are by virtue of the thermal wind balance related to meridional temperature gradients. Therefore, the upper and lower-level temperature trends are thus engaged in a tug-of-war around the future evolution of the jet stream and its associated storm track (Shaw et al. 2016).

Besides forced trends, storm tracks and eddy-driven jets exhibit substantial temporal and spatial variability (Hartmann 2007). Their activity is larger during winter when the equator-to-pole temperature gradient is higher and consequently the energy transport is more intense compared to summer. A remarkable exception to this behaviour is found in the North Pacific, where storm activity is lower in mid-winter (Nakamura 1992; Schemm and Rivière 2019; Schemm et al. 2021). The position of the storm tracks has also a seasonal cycle whereby storm tracks and jet streams are located at lower latitudes during winter. Furthermore, they display high frequency variations in intensity and position from shorter time scales of the order of weeks, related to oscillatory behaviour of the regime life cycle produced by consumption and replenishment of baroclinicity, to multidecadal variations. Indeed, storm tracks can be affected by tropical variability across different scales, from sub-seasonal scales produced by the Madden-Julian Oscillation (Yadav and Straus 2017) to decadal variations generated by El Niño-Southern Oscillation (Eichler and Higgins 2006; Schemm et al. 2018) and multidecadal variability (Bracegirdle et al. 2018).

Jet stream trends are therefore affected by both the impacts of anthropogenic warming on circulation and natural variability. Previous studies based on reanalysis data have found strong

seasonal and regional variations in jet changes over the past decades with limited robust trends in wind speed or position (Manney and Hegglin 2018) and in particular for the subtropical jet no robust poleward trends have been identified in reanalyses (Maher et al. 2020). Simmons (2022) reported an intensification and equatorward shift of the jet stream over the eastern North Atlantic related to a warming minimum between Greenland and Europe in the ERA5. Martin (2021) found increased waviness of the eddy-driven and subtropical jets and a poleward shift of the eddy-driven jet while Woollings et al. (2023) highlighted the role of upper tropospheric warming to explain the poleward shift of jet streams in both hemispheres, but dit not look at the North Atlantic region in particular.

Climate model projections exhibit large uncertainty concerning the future of the wintertime eddy-driven jet on the North Atlantic compared to the jets over other ocean basins (Simpson et al. 2014; Lorenz and DeWeaver 2007; Woollings 2010), which is potentially linked to the nature of the North Atlantic as a mostly eddy-driven jet stream (Lee and kyung Kim 2003; Li and Wettstein 2012). These uncertainties have a strong influence on the low confidence in future changes in the hydrological cycle and the occurrence of extreme wind events, since the vast majority of heavy precipitation and intense wind events during the cold season are associated with extratropical cyclones (Pfahl and Wernli 2012; Owen et al. 2021). For Europe, which lies at the end of the North Atlantic storm track, changes in the jet stream and storm tracks are thus particularly relevant. Therefore, future European rainfall and wind will be significantly affected by the direction and magnitude of any meridional shift in the storm track and/or position of the jet stream (Priestley and Catto 2022). Currently, it is only settled that sea surface temperatures (SST) and their influence on low-level baroclinicity account for a fraction of the change (Woollings et al. 2012) but the interplay between changes in baroclinicity, diabatic heating, storm tracks and the jet stream and the chain of processes that explain past changes in the North Atlantic jet stream have not been clearly established.

The atmospheric response to increased diabatic heating is relevant to understand changes in the North Atlantic jet. In this regard, Peng and Whitaker (1999) investigate the response to diabatic heating by using a linear baroclinic model, which is a primitive equation model linearized about a basic state including heating and eddy terms as forcing. The response consists of a low-level trough, whose extension depends on the heating distribution, and an upper-level ridge downstream. The

imposed heating is interpreted as the initial heating before the atmosphere has adjusted to it. The resulting anomalous flow is inserted into to a linear storm track model, which is a quasigeostrophic model linearized about a time-mean flow[1] to deduce the anomalous eddy forcing, which in turn is re-inserted into the linearized baroclinic model to obtain the eddy-driven anomalous flow. By doing so, the baroclinic response to diabatic heating evolves to an eddy-driven response with a barotropic structure and finally to a net flow response (initial heating response plus eddy feedback) of the North Pacific storm track. For a background state inspired by the January climatology, they show that the eddy forcing acts to shift the heating-induced anomalous ridge downstream and toward the northeast.

More generally, several mechanisms can affect the mean jet position and intensity in the presence of diabatic heating acting on different time and spatial scales:

First, a large fraction of the diabatic heating on the scale of individual eddies is generated along ascending airstreams in the warm sector of extratropical cyclones, known as warm conveyor belts (Harrold 1973; Browning et al. 1973). As shown in Sheldon et al. (2017), the warm conveyor belt activity at the entrance of the Atlantic storm tracks is anchored above the warm tongue of the Gulf Stream and could explain the co-location between time-mean ascents, precipitation and the warm tongue (Minobe et al. 2008). Warm conveyor belts can have a local influence on the jet. Diabatic heating produces a positive potential vorticity (PV) anomaly at low levels and a negative PV anomaly near the tropopause (Stoelinga 1996; Pomroy and Thorpe 2000), which is schematically represented in Fig. 4a from Wernli and Davies (1997). Such PV anomaly can locally intensify the jet (Grams et al. 2011; Schemm et al. 2013; Weijenborg and Spengler 2020; Rivière et al. 2021; Wimmer et al. 2022).

Second, the North Atlantic jet stream is driven by eddy momentum flux convergence associated with the propagation of large-scale Rossby waves that originate from regions of enhanced baroclinicity (Hoskins et al. 1983; Vallis 2017), suggesting a strengthening of the eddy-driven jet if baroclinicity increases. In this regard, the presence of oceanic frontal areas, such as the Gulf Stream, has been shown to be crucial to maintain the baroclinicity through sensible heat fluxes (Sampe et al. 2010; Hotta and Nakamura 2011). Further, it has been established that not only is an increase in baroclinicity important, but its the exact location relative to the mean jet position

[1]The authors note that the time-mean flow was taken from the eastern North Pacific, which during winter is dominated by the subtropical jet stream, while the model appears to be too sensitive to the forcing when using the time mean conditions from the North Atlantic, which has more the nature of an eddy-driven jet.

matters (Rivière 2009). An increase of baroclinic eddy activity can thus lead to an acceleration or shift of the jet but also entails an enhanced diabatic heating associated with the growing baroclinic eddies that maintains the storm track (Hoskins and Valdes 1990a).

Quantifying the relevance of each of these mechanisms and their effects on the jet is therefore necessary to understand changes in the North Atlantic jet stream. We aim at investigating the role of changes diabatic heating in recent changes of the jet stream through the analysis of ERA5 data for the winter season following the above outlined two mechanisms. To this end, next to ERA5, a hierarchy of idealized and fully-coupled climate simulations is used to better understand the relevance of diabatic heating and mean baroclinicity on the trends in the winter North Atlantic circulation. This analysis also allows us to pinpoint to potential sources of uncertainty in climate projections, and provide some guidance on relevant aspects required to adequately simulate jet stream changes that most models do not adequately capture (Blackport and Fyfe 2022). Admittedly, additional processes, such as stratospheric (Kidston et al. 2015) or tropical influences (Yu and Lin 2016), may play a role in jet trends, but this study mainly focuses on the impact of changes in diabatic heating. It should also be noted that this study does not attempt to attribute trends to either natural variability or anthropogenic climate change.

Specifically, this study addresses the following research questions:

- What is the local effect on the jet of an increase in transient diabatic heating rate pulses over the storm track entrance region resulting from enhanced diabatic heating on the scale of individual cyclones (as, for example in Fig. 4a, in Wernli and Davies 1997)?

- What is the downstream impact of a change in mean baroclinicity, potentially resulting from enhanced diabatic heating over the Gulf Stream sector, on the downstream evolution of the North Atlantic jet via eddy momentum flux convergence (as, for example, in Hoskins et al. 1983)?

- Which of these processes are adequately represented in fully-coupled climate simulations and what are the factors that contribute to uncertainty in climate projections of the North Atlantic jet stream?

The remaining of the paper is structured as follows. Section 2 presents the winter North Atlantic jet trends in the reanalysis and illuminates the main mechanisms driving the trends,

Section 3 discusses the local effect of diabatic heating over the Gulf Stream through an idealized frontal-geostrophic model experiment, Section 4 explores the role of feedback of eddy horizontal momentum fluxes onto the mean flow through aquaplanet simulations and Section 5 analyzes jet trends in fully-coupled climate simulations. Main conclusions are provided in section 6. To improve readability of the individual sections, the main data and methods are introduced in the corresponding sections.

2. Observed jet stream trends over the North Atlantic

The ERA5 reanalysis (Hersbach et al. 2020) is used to evaluate recent trends in the winter (December–February, DJF) North Atlantic jet stream. The dataset consists of global data with a spatial resolution of 0.28° and 137 vertical levels up to 1hPa, spanning from 1979 until present with hourly temporal resolution. For the analysis presented in this study horizontal wind components and temperature were interpolated into an horizontal resolution of 0.5° and 11 pressure levels between 900 and 100 hPa[2]. Linear trends are computed from daily averages in the period 1979-2022. This data frequency is considered to be representative enough for the subsequent trend analysis. Although ERA5 reanalysis data are available from 1940, the period is restricted to the satellite era. This is because the main region of interest is the North Atlantic and thus the reanalysis may not be well constrained over the ocean in the earlier period. However, zonal wind speed trends for the period before the satellite era are provided in Appendix A.

a. Methods to analyze trends

1) Baroclinicity: Isentropic slope

To study the impact of changes in baroclinicity in the modification of the jet stream, we use the slope of the isentropic surfaces to quantify the growth potential of baroclinic waves, such as extratropical cyclones (Van Delden 1999; Thompson and Birner 2012; Igel and van der Heever 2014; Papritz and Spengler 2015). A necessary condition for baroclinic growth of a disturbance is that on average the motion of air parcels has a slope lower than the slope of the isentropic surfaces

[2]The following pressure levels in hPa are used in this study: 100, 200, 250, 300, 400, 500, 600, 700, 800, 850 and 900.

(Green 1960). The slope is computed as

$$S = \frac{\frac{\partial \theta}{\partial y}}{\frac{\partial \theta}{\partial p}}, \tag{1}$$

where θ is the potential temperature, y represents the meridional direction and p is pressure. The slope is computed from hourly data averaged to obtain daily means, which are used to compute linear trends.

2) Eddy momentum flux convergence: E-vector

Eddy momentum convergence is explored by means of the divergence of the E vector (Hoskins et al. 1983), whose direction indicates eddy propagation, which is opposite from the eddy momentum transfer. The three-dimensional E vector is defined as

$$\mathbf{E} = \left(0.5\,\overline{(v'^2 - u'^2)}, -\overline{u'v'}, \frac{f}{\partial\theta/\partial p}\overline{v'\theta'}\right), \tag{2}$$

where u and v are the zonal and meridional wind components, respectively, f is the Coriolis parameter and p is pressure. The overbars indicate time means and the primes denote anomalies, which are computed by subtracting the 10-day high pass filtered component from the total fields. The vertical component of the E vector is thus proportional to the heat flux.

The orientation of the E vector is related to the eddy shape and the orientation of Rossby wave breaking (RWB) (Orlanski 1998). Equatorward E vectors indicate anticyclonic RWB, while cyclonic RWB is associated with poleward E vectors (Drouard et al. 2015). Additionally, the zonal component of the E vector provides an indication of the eddy shape, so meridional elongated eddies are represented by eastward E vectors and zonally elongated eddies by westward E vectors. 6-hourly data are used to compute the E vector, which is subsequently daily averaged.

3) Statistical significance

We apply the false-discovery rate (Wilks 2016) to compute p-values for the trends computed throughout the study. With this approach, a global p-value, p^* defined by: $p^* = max[p_i \leq (i/N)\alpha]$ is computed, where i is the index identifying the sorted p-values, N is the total number of grid

points and α is a threshold that controls the fraction of null hypotheses erroneously rejected, which is fixed to 0.1 in this study. For each grid point, local p-values are compared to the global p-value.

b. Observed jet stream trends over the North Atlantic

Analysis of the wintertime (December-January-February) zonal wind speed trend in the ERA5 dataset from 1979 until 2022 shows a strengthening and mild poleward shift of the North Atlantic jet stream between 40°N and 50°N (Fig. 1a) over the entrance of the storm track on the US East Coast and the Gulf Stream sector (Fig. 1b). This is not the case further downstream over the eastern North Atlantic, where the trend is characterized by a slight equatorward shift and a southwest-to-northeast extension towards the UK and western Europe. There is also a decrease in zonal wind speed between 20–30°N, extending towards the Iberian Peninsula and the western Mediterranean (Fig. 1b), and an additional decrease north of the jet between 65–80°N over the Nordic Seas.

Upstream over eastern North America, the trend in the 500-hPa geopotential anomalies shows an intensification of the climatological trough over North America (dashed green contours in Fig. 1b). At lower levels, the negative anomaly extends to the east, indicating the presence of a westward tilted trough with height. The implications of this pattern are discussed in the next subsection.

1) Trends in potential temperature, diabatic heating and temperature advection

We begin the detailed analysis of the jet trends by investigating the mechanisms that affect it over the Gulf Stream before consideration is given to the downstream sector over the eastern North Atlantic. We first perform a trend analysis of the potential temperature and changes in its meridional structure related to diabatic heating and advection. Figure 2 presents trends in potential temperature, diabatic heating[3] and three-dimensional potential temperature advection tendency. The general trend in potential temperature depicts enhanced potential temperature between 30–40°N, slightly equatorward of the region of increased zonal wind speed and 80–90°N (red shading in Fig. 2a,b). The increase located near the pole is seemingly associated with the Arctic Amplification (AA). It reaches into the stratosphere (Fig. 2a).

At midlatitudes between 30-50°N potential temperature increases in the troposphere but decrease in the stratosphere, leading to a decrease in static stability (Fig. 2a) in the layer between 350–200 hPa,

[3]Diabatic heating refers to the sum of the potential temperature tendencies due to radiation, turbulence, convection, the microphysics of clouds and the drag of gravity waves from the physical model underlying the reanalysis data.

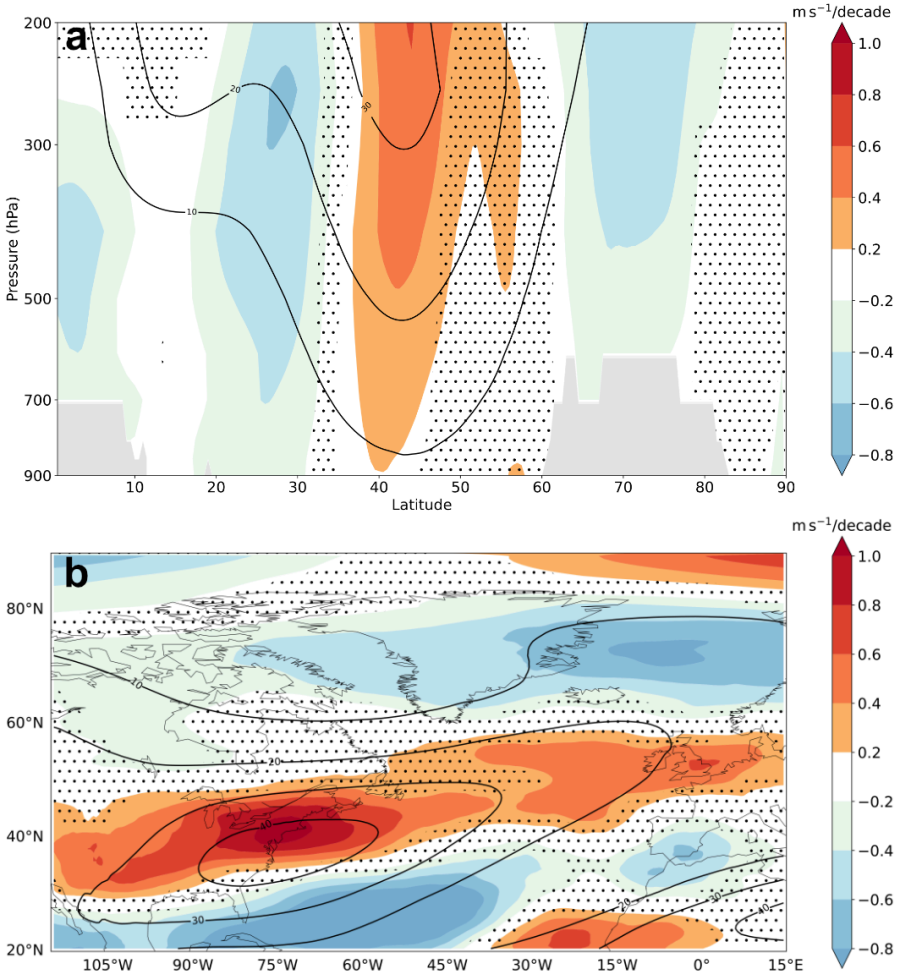

239 FIG. 1. **Wintertime zonal wind speed trend over the North Atlantic in ERA5:** a) Mean of the trend
240 (shading) and climatological average in zonal wind speed (black contours) over the North Atlantic storm track
241 region (80°W – 15°W) for DJF in the period 1979-2022. b) Zonal wind trend (shading) and climatological mean
242 (black contours) at 250 hPa. The stippling represents areas with p-values higher than p^* (see text for details).

255 exactly where the tropopause height increases (light blue contours in Fig. 2a indicate the dynamical
256 tropopause during the first and last decades).

271 To better understand the trend in potential temperature, it is illustrative to analyze changes
272 in diabatic heating, which are described above, and advection, as both processes locally affect
273 potential temperature. Although attributing trends to either anthropogenic climate change or natural
274 variability is beyond the scope of this study, it is appropriate to analyze trends in diabatic heating
275 and advection in light of changes in a warmer climate and how these may affect baroclinicity. Moist

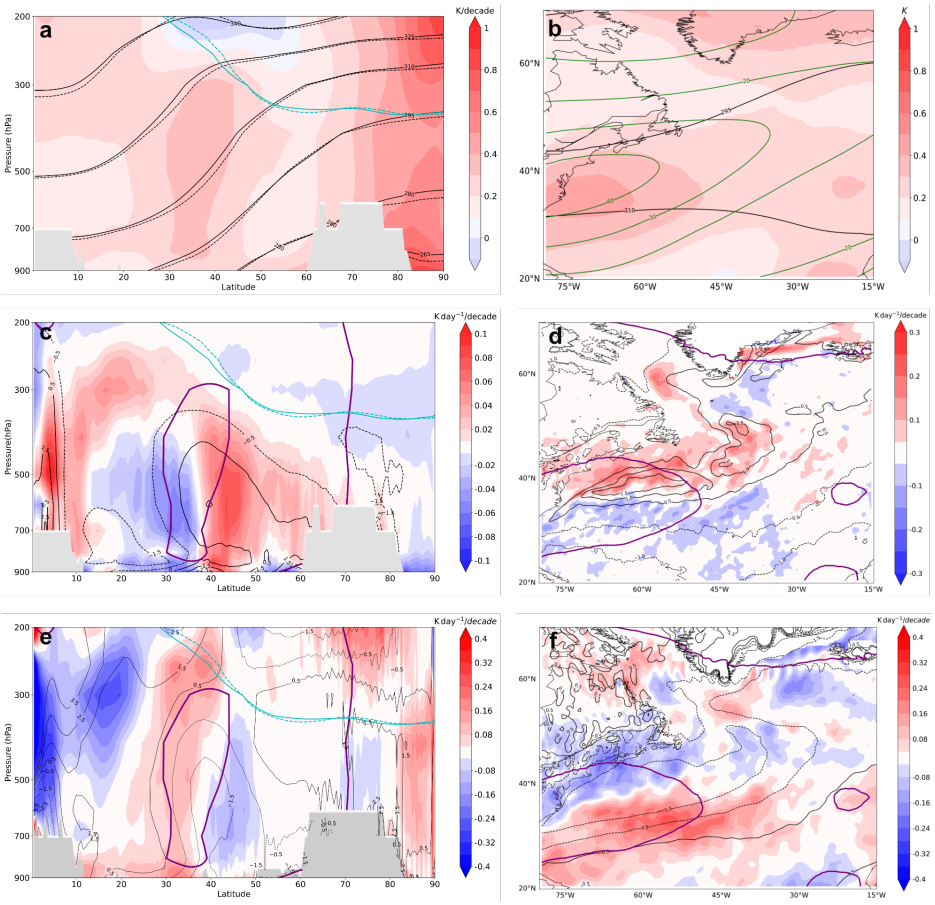

FIG. 2. **DJF Potential temperature, diabatic heating and advection trends over the North Atlantic:** a) Zonal mean of the potential temperature trend between 80°–15°W (shading), zonally averaged potential temperature mean in the same sector for the first (solid black lines) and the last decade (dashed black lines) in the selected period for ERA5 (1979-2022). b) Trends in potential temperature (shading) and climatological mean (black contours) averaged between 300 and 850 hPa. Green contours represent zonal wind speed climatology in the ERA5 period at 250 hPa. c) Zonal mean of the trend in potential temperature tendency due to parameterizations (diabatic heating) between 80°–15°W (shading). Black contours depict the climatological mean. d) Trends in diabatic heating (shading) and climatological mean (black contours) averaged between 300 and 850 hPa. e) Zonal mean of the trend in potential temperature tendency due to three-dimensional advection in the same North Atlantic sector. Black contours show the climatological mean over the same region. f) Trends in potential temperature tendency due to advection over the North Atlantic averaged between 300 and 850 hPa (shading) and climatological mean (black contours). In panels a), c) and e) solid and dashed light blue contours depict the 2-PVU potential vorticity contour for the first and last decades in the ERA5 data, respectively. In panels c)-f) the contour corresponding to a potential temperature trend of 0.3 K/decade is represented by purple lines.

diabatic processes are expected to increase in a warmer climate, as the saturation vapor pressure of the atmosphere increases with rising temperatures – as a result of the Clausius-Clapeyron relation (Held and Soden 2006) –, thus increasing potential temperature locally, while a reduction in the land-sea contrast has the potential to promote a reduction in cold-air advection into the region of interest from upstream (Wallace and Joshi 2018), thus also increasing the potential temperature over the Gulf Stream area.

In the Gulf Stream sector, ocean fronts have been shown to intensify the storm track (Small et al. 2014). In addition, this is an area of enhanced upward motion and cloud formation (Minobe et al. 2008; Kuwano-Yoshida et al. 2010), it is thus expected that diabatic heating plays climatologically an important role. Indeed, the climatological mean diabatic heating (black contours in Fig. 2c,d) is co-located with the mean position of the Gulf Stream. The trend pattern displays a dipolar structure in a meridional band between 20–60°N (shading in Fig. 2c,d) with an increase near its climatological mean position (black solid contour in Fig. 2d) and a slight poleward shift plus a reduction south of 40°N, where it is climatologically negative (dashed black contour in Figs. 2c,d). The trend pattern suggests a mild poleward shift paired with an intensification of diabatic heat release close to its climatological maximum value.

Ambaum and Novak (2014) and Novak et al. (2015) show that the time series of diabatic heating over the Gulf Stream region is characterized by spikes that occur on synoptic time scales and are indicative of the baroclinic development growth of extratropical cyclones. These results and the linear upward trend in diabatic heating suggest that the diabatic heat release for each, or at least some of these events, has increased over recent decades. The trend in the jet over the Gulf Stream likely reflects the cumulative influence of many of these diabatic heating peaks of increasing intensity, the net effect of which is a local strengthening and regionally limited poleward shift of the jet. To quantify this increase in strong peaks of diabatic heating, Fig. 3 compares the values of the percentiles in the distribution of diabatic heating in an area near the Gulf Stream for the first and last decades of the ERA5 period. In the last decade, the values of the highest percentiles are larger than in the first decades, which supports the argument of increased intensity in the strongest diabatic heating pulses. To illuminate this diabatic heating-jet stream interactions, an idealized two-dimensional frontal-geostrophic simulation is used in Section 3 to estimate the effect a single

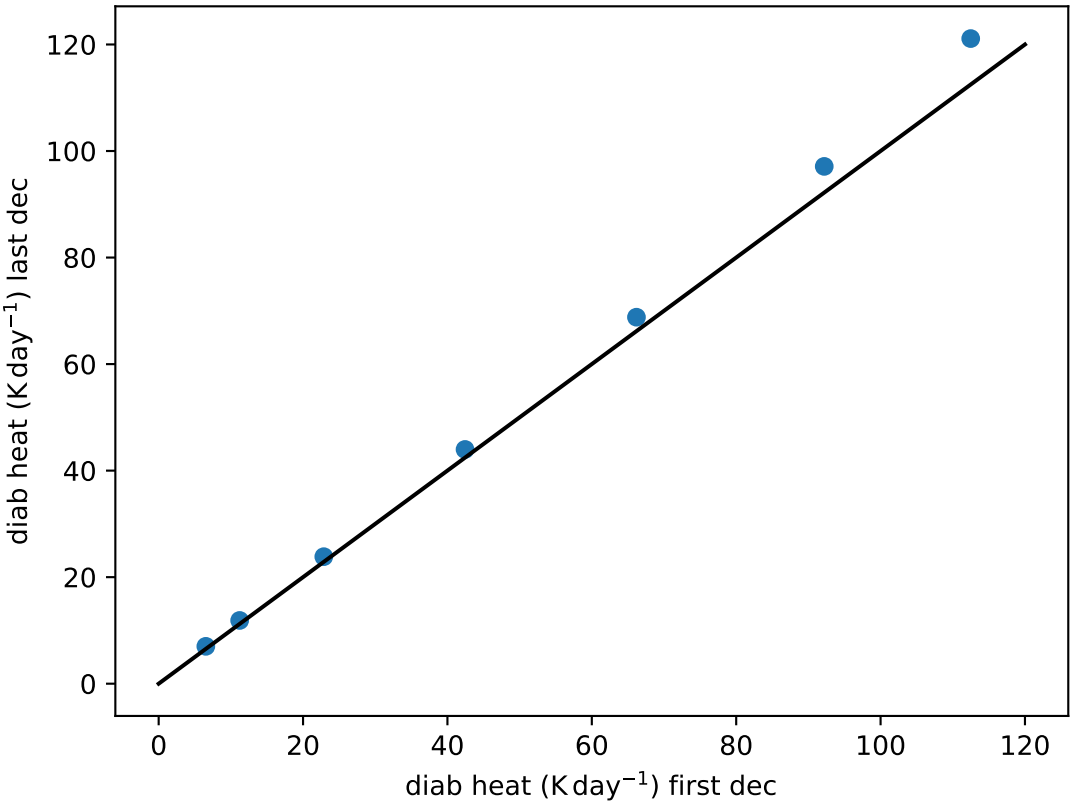

FIG. 3. **Quantile-quantile plot for the diabatic heating:** Values of diabatic heating percentiles in the area between 80–30°W, 35–45°N and 300–850 hPa for the first decade (horizontal axis) and last decade (vertical axis) in the considered ERA5 period (1979-2022). The lowest value corresponds to percentile 90 and the highest to percentile 99.9999. The black line represents the reference corresponding to equal values of the percentiles for both decades.

diabatic heating event has on the position and strength of an idealized jet stream and whether it produces an impact comparable to the observed jet feedback over the Gulf Stream sector.

Fig. 2e,f display advection trends in ERA5 data. In this case, there is a positive trend between 20–35°N with a low vertical tilt over the US East Coast – Gulf Stream region (red shading in Fig. 2e,f). This positive trend in the potential temperature advection is dominated by an upward trend in zonal advection. Because advection north of 25°N is climatologically negative (dashed black contours in Fig. 2b,d) the upward trend indicates a reduction in cold-air advection. This effect may be related to a reduction in the winter land-sea temperature contrast, as warming is more pronounced over North America than over the adjacent ocean (see Fig. 3a in Simmons (2022)).

Although the positive advection trend is also strong at upper levels, the positive signal extends towards the surface supporting the role of reduced land-sea contrast as a driver of this trend. The maximum in potential temperature trend between 30–35°N is well aligned with the reduction in cold advection. This suggests that advection is the main contributor to the potential temperature trend in this region. Between 35 and 40 °N, the maximum in potential temperature trend coincides with the positive trend in diabatic heating, especially at mid and upper levels (Fig. 2c).

2) Trends in mean baroclinicity

Next, we analyze changes in baroclinicity, especially over the downstream sector. By thermal wind balance, the baroclinic component of the jet increases where the horizontal temperature gradient is stronger. Fig. 4 reveals a tripolar trend pattern in the isentropic slope, which is used as a proxy for the mean baroclinicity, over the North Atlantic storm track (see subsection 1). There is a positive trend in midlatitudes, between 40–50°N (red shading in Fig. 4a) flanked by two bands of negative trends. The upper-level maximum of the increase is located at 300 hPa around the main jet axis, close to where an increase in the zonal wind speed (Fig. 1a) is identified. The combination of a reduction in upper-level static stability, coupled with an increase in the meridional temperature gradient, leads to this increase in mean baroclinicity in the 40–50°N band, which appears to be critical for the evolution of the North Atlantic jet in this sector. This is accompanied by a lifting of the dynamical tropopause near 40°N (light blue solid and dashed contours in Fig. 4a). In the middle and lower troposphere, the slope trend shows a decrease equatorward of the jet axis at 30°N, and an increase around the mean jet axis and again a decrease in a latitude band between 50 °N and 80°N (Fig. 4a). Trends in slope, potential temperature and diabatic heating are consistent. The region of strongest increase in potential temperature is related to a combination of reduced cold-air advection in the equatorward flank of this area and a positive trend trend in diabatic heating, which is located polewards of the increase in advection. In a baroclinic atmosphere a diabatic heating maximum tends to lower the height of a tilted isentropic surface on its equatorward side and a lowered isentrope corresponds to an increase in potential temperature (Van Delden 1999; Papritz and Spengler 2015). This pattern in combination with the reduced cold air advection results in the increase in potential temperature (Fig. 2a,c), which is found slightly equatorward of the increase in the slope (Fig. 4) and diabatic heating release (Fig. 2c,d). At high latitudes, the warming pattern

(Fig. 2a,c) causes the isentropic surfaces to bend downward causing a lowered slope at equatorward latitudes and an increased slope at even higher latitudes, which is in agreement with the dipole trend pattern of the slope between 70–90°N (Fig. 4a). Overall, the slope trend is strongest between 40–50°N, which is close to its climatological mean position, and it extends throughout the entire troposphere (Fig. 4a).

3) Trends in eddy momentum flux

Finally, we analyze trends in eddy momentum convergence by means of the E vector. The direction of horizontal momentum flux is opposite to the direction of the meridional E vector. Therefore, increased eddy momentum convergence is represented by a larger E vector divergence. The axis of zero E vector divergence is located around 45°N and eddy momentum convergence peaks slightly north of the jet core over eastern North America (vectors and shading in Fig. 5), which is in agreement with the intensification and northward shift of the jet in this sector (Fig. 1b) and the area of positive slope trend (Fig. 4b). Downstream over the eastern North Atlantic, momentum convergence is enhanced south of the climatological jet position, where an intensification, a mild equatorward shift and an extension of the jet are identified. In general, the area of increased momentum convergence coincides well with the region where the jet intensifies (Fig. 1b), consistent with the general understanding that the North Atlantic jet is an eddy-driven jet. The enhanced convergence of the eddy momentum flux near the jet axis and a reduction poleward of the climatological jet flank produces a reduction of the jet width, which agrees with analyses of the projected trends of the North Atlantic jet (Peings et al. 2018). Overall, the momentum trend pattern is remarkably similar to the archetypal steering of Rossby waves by baroclinic eddies, in particular over the western North Atlantic and the storm track entrance region. Momentum convergence is enhanced in the area of steering and waves propagate meridionally away from this region (Vallis 2017). In addition, over the western North Atlantic, upper-level changes in the eddy momentum flux convergence are related to a trend towards more poleward-oriented E vectors. This change in E vector is indicative of enhanced cyclonic RWB, which contributes to the equatorward shift of the downstream where waves typically break. The intensification of the climatological trough provides a potential explanation for the asymmetry of the E vector trend. Downstream of a trough anomaly,

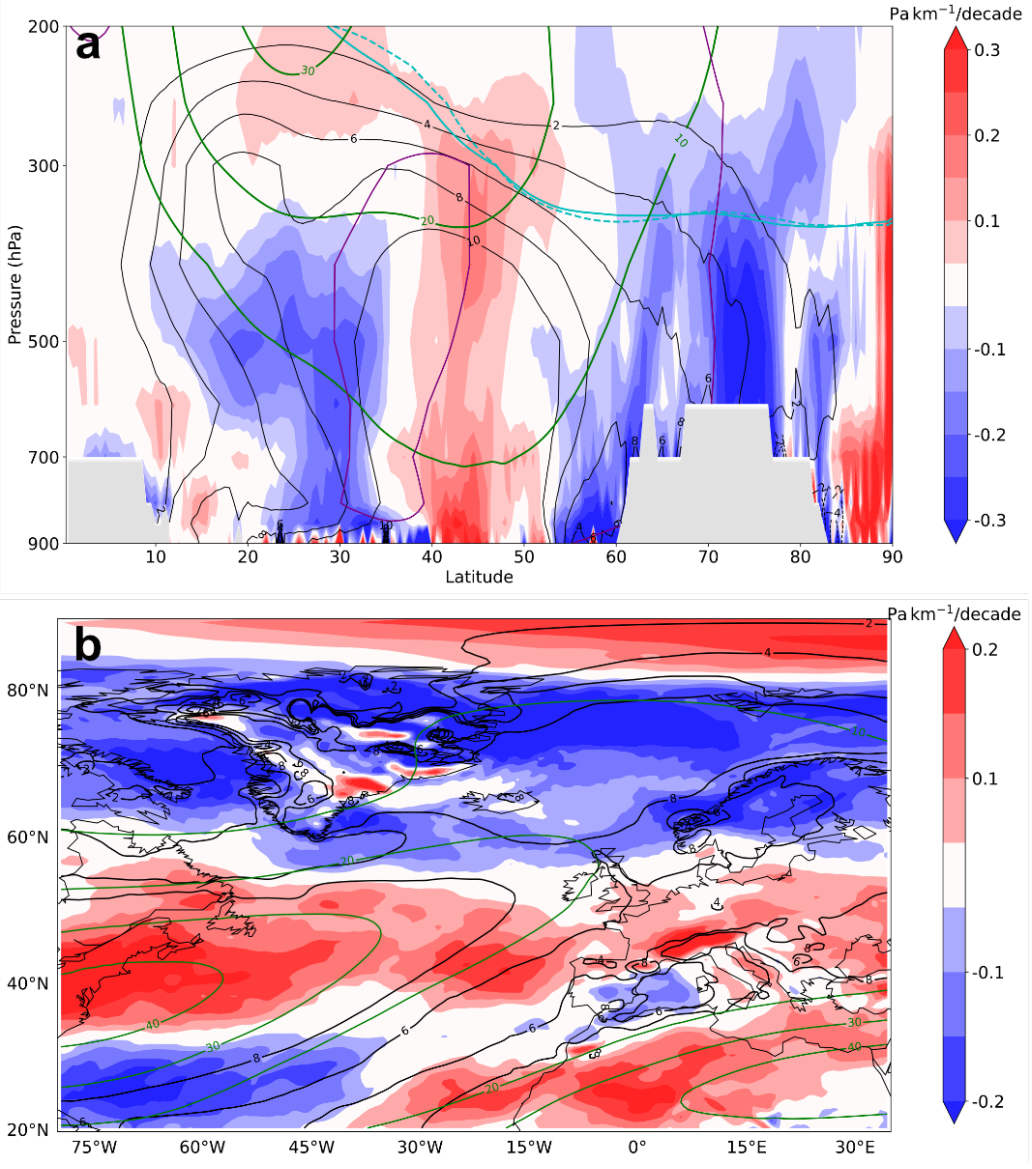

FIG. 4. **DJF isentropic slope trends in ERA5 over the North Atlantic:** a) Zonal mean of the trend in the slope of the isentropic surfaces between 80° – 15°W (shading), climatological mean slope (black contours, in Pa km^{-1}) and zonal mean zonal wind (green contours) in ERA5 (1979-2022). Blue contours represent the tropopause height (2 PVU contour) for the first (solid) and last decade (dashed) in the considered period. For reference, the contour corresponding to a potential temperature trend of 0.3 K/decade is represented by purple lines. b) Trend of the slope of the isentropic surfaces averaged between 250 and 850 hPa (shading), climatological mean over the same vertical layer (black contours) and climatological mean zonal wind speed at 250 hPa (green contours).

upper-level transient eddies tend to propagate with a cyclonic orientation, which is associated with poleward pointing E vectors (Drouard et al. 2013).

At the same time, the vertical component of the E vector, which is proportional to the meridional eddy heat flux, displays an upward trend between 40–50°N below 700 hPa (Fig. 5a). The upward E vector in the lower troposphere indicates an increase in the initial growth of eddy activity at the entrance region of the storm track. The anomalous E vector diverges in the upper troposphere from the same latitudes where eddy activity increases, consistently with well-known storm-track properties (see Fig. 13 in Hoskins et al. (1983)). Additionally, eddy heat flux is also reduced below 400 hPa at high latitudes. This is associated with a decrease of the meridional near-surface temperature gradient in this sector due to the Arctic Amplification. This also suggests that the influence of the AA on the activity of the transient waves is limited to high latitudes north of approximately 70°N.

The zonal component of the E vector is also reduced over the western North Atlantic between 75–60°W, 45–50°N (Fig. 5b). The zonal E vector component tends to cause a southwest–northeast tilting of the storm track (see Fig. 3 in Orlanski (1998)), as a result of the quadruple vorticity pattern associated with the zonal E vector component. Therefore, this reduction implies a reduced northward deflection of the jet (Orlanski 1998) and thus, a more zonal orientation of the storm track. The reduction in the zonal component of the E vector could explain the zonal extension over the eastern North Atlantic and indicates changes in eddy shape, that is, a tendency towards less meridionally and more zonally elongated eddies (Orlanski 1998).

In summary, over the western North Atlantic and the storm track entrance region, where diabatic heating intensifies, the jet strengthens and shifts slightly poleward, while over the eastern North Atlantic it intensifies, extends downstream, shifts slightly equatorward and tends to become more zonal. Established theoretical considerations based on a linear wave model suggest that an increase in diabatic heating is inherently connected to the formation of a westward tilted trough, which at lower levels is located downstream of the maximum in heating (Hoskins and Karoly 1981). This effect is not reproduced in the reanalysis (not shown) and this discrepancy could be related to the role of nonlinearities in the response.

An increase in the mean baroclinicity over the Gulf Stream sector affects the entire depth of the troposphere and an increase of the convergence of eddy momentum fluxes in a zonal band across the

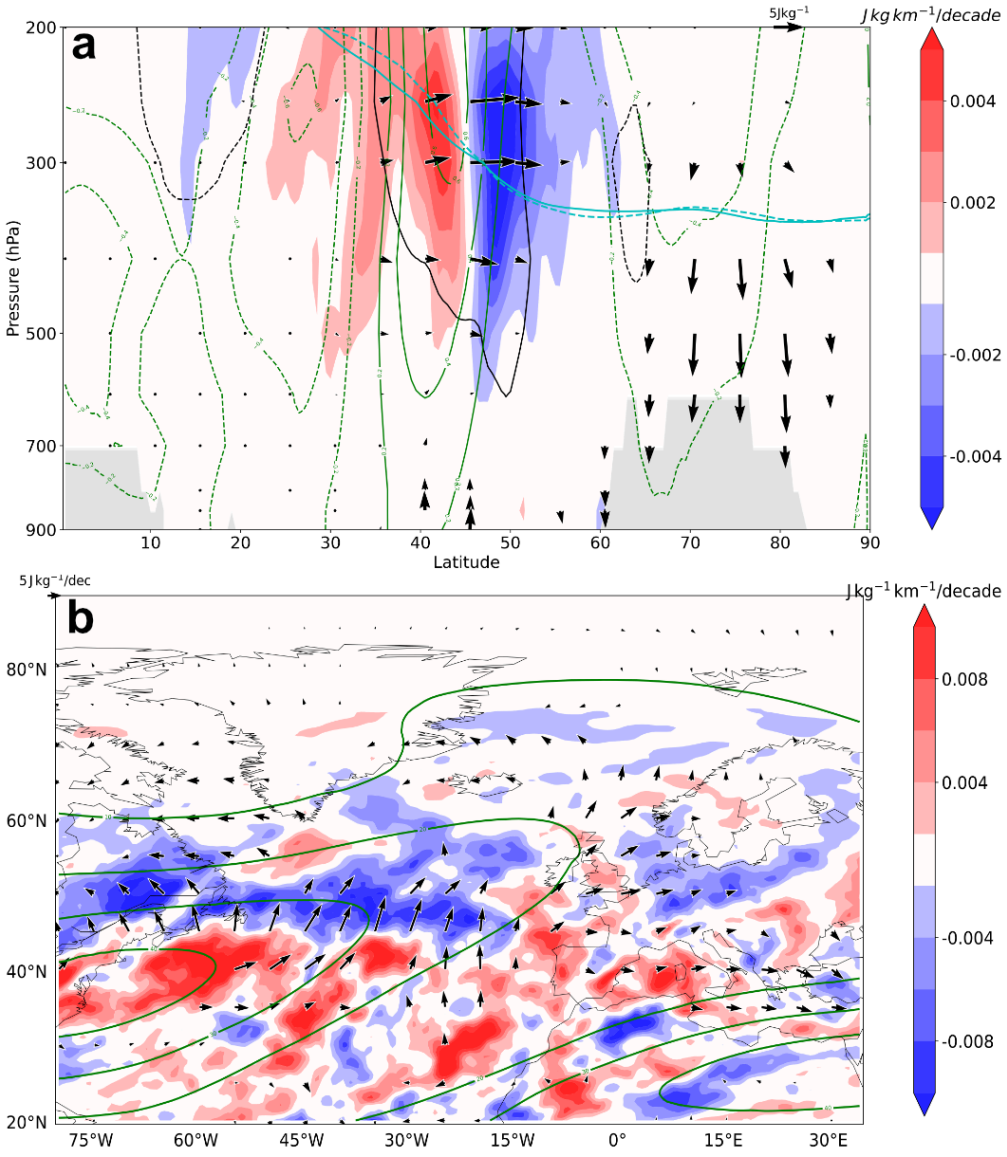

FIG. 5. **DJF E vector trends in ERA5 over the North Atlantic:** a) Zonal mean of E vector divergence trend over the North Atlantic sector, between 80°–15°W (shading), climatological mean over the ERA5 period in DJF (black contours, $\pm 10^{-5}$ Jkg^{-1}m^{-1}) and trend in zonal wind speed (green contours). Black vectors represent E vector trend (per decade). The size of the vertical component is four times the size of the horizontal component. Blue contours represent the tropopause height (2 PVU contour) for the first (solid) and last decade (dashed) in the considered period. b) E vector trend (black vectors) and divergence trend (shading) in ERA5 (1979-2022) at 250 hPa over the North Atlantic. Green contours represent the climatological mean of the zonal wind at the same pressure level. In both panels, vectors are shown only if the p-value in at least one of the components is lower than the global p^*.

entire North Atlantic is suggestive of an acceleration of the jet through the excitation of baroclinic waves. In addition, a northward trend in the E vector suggests an increase in cyclonic wave breaking, which contributes to the equatorward shift of the jet downstream. In the next sections, the local influence of diabatic heating over the Gulf Stream as well as the downstream mechanism related to the eddy-mean flow interaction are further explored through idealized simulations.

3. Local diabatic influence on the jet stream

a. Two-dimensional frontal-geostrophic simulation

At the jet entrance above the east coast of North America and the Gulf Stream sector, the jet latitude is less variable compared to the central and eastern North Atlantic (Brayshaw et al. 2011; Small et al. 2014; O'Reilly et al. 2017). In this sector, rapid growth of baroclinic waves is occurring due to high baroclinicity. Additionally, diabatic heating in the lower to mid troposphere, which occurs episodically within baroclinic wave development (Ambaum and Novak 2014), is known to have a local impact on the jet stream through the modification of PV (Stoelinga 1996; Pomroy and Thorpe 2000) in an environment characterized by strong vertical wind shear beneath the jet stream core. The purpose of this section is to quantify this direct and transient effect of a repeated increase in diabatic heating during baroclinic wave development by using a two-dimensional frontal-geostrophic model (Harvey et al. 2020) including an idealized diabatic heating perturbation inspired by the trends obtained in ERA5 (Figs. 6 and 2c). It is expected a PV reduction above the heating and an increase below, which are associated with circulation changes that locally affect the jet (Wernli and Davies 1997).

The two-dimensional frontal-geostrophic model is based on the elliptic Sawyer-Eliassen equation, including diabatic heating, under the Boussinesq approximation (Harvey et al. 2020). The model is initialized with zonal wind and potential temperature profiles similar to the ERA5 climatology in the Gulf Stream sector (Fig. 6) and a Gaussian diabatic heating perturbation, which remains constant during the whole simulation period and has a maximum of approximately 0.4 Kday^{-1}, which matches the maximum in the long-term trend in ERA5. This perturbation is designed to mimic the average rate of increased local diabatic heating in the Gulf Stream sector, as identified in the long-term trend in ERA5. This experiment aims to establish whether the magnitude of the increase in zonal wind in this area detected in the reanalysis trend is consistent with the effect of

a succession of intensified diabatic heating pulses during the development of individual cyclones. For heights between approximately 2 and 7 km the heating is greater than 0.1 $\mathrm{K\,day^{-1}}$ (Fig. 6). Additional experiments with an extended region of heating reaching lower levels as obtained for the trends in ERA5 (Fig. 2c) produce qualitatively similar results.

In more detail, the model is integrated forward in time while PV is positive over the full domain, which is a necessary condition for the Sawyer-Eliassen equation to be elliptic. It typically takes four to five days, given the magnitude of the diabatic heating rate imposed, before the forcing drives the PV negative above the heating maximum. This is longer than typical synoptic timescales and so we would expect in practice that the heating in each system would stop earlier as a baroclinic wave life cycle follows its course. The model evolves by advecting the full Ertel PV field, which under the two-dimensional Boussinesq assumptions reduces to $P(y,z) = (m_z\theta_y - m_y\theta_z)/\tilde{\rho}$ where zonal angular momentum $m = -fy + u$ and $\tilde{\rho}$ is the background density, in the meridional (y,z) plane. The (v,w) wind are obtained from the Sawyer-Eliassen equation assuming no normal flow at the domain boundaries. The resulting (u,θ) fields are obtained by inverting P using a two-dimensional Monge-Ampère solver, together with boundary conditions $u = 0$ on the meridional boundaries ($\pm$3000 km), $\theta' = 0$ on a rigid lid (16 km) and a time-varying lower-boundary condition $\lambda(y) = -\theta m_y$. This form of the lower boundary condition is analogous to advecting boundary θ in the quasi-geostrophic equations, whilst maintaining the compatibility condition required for solution of the two-dimensional Monge-Ampère equation.

This experiment has some similarities with the first step in the study of Peng and Whitaker (1999), where a linear three-dimensional baroclinic model is used to investigate the response to an initial anomalous heating (before adjustment and eddy feedback). However, the approach used here is based on a two-dimensional nonlinear model and our interpretation is that it is the local response of the jet structure to transient heating beneath the level of the jet maximum over the Gulf Stream. Our 2D model cannot develop troughs and ridges, a mechanism which we explore with a non-hydrostatic global atmospheric model in an aquaplanet configuration in another section.

b. Experiment results

The results of the simulation show an intensification of the zonal wind, whose maximum exceeds 2 $\mathrm{m\,s^{-1}}$ and a slight poleward shift of the jet above the area of increased diabatic heating (Fig. 7).

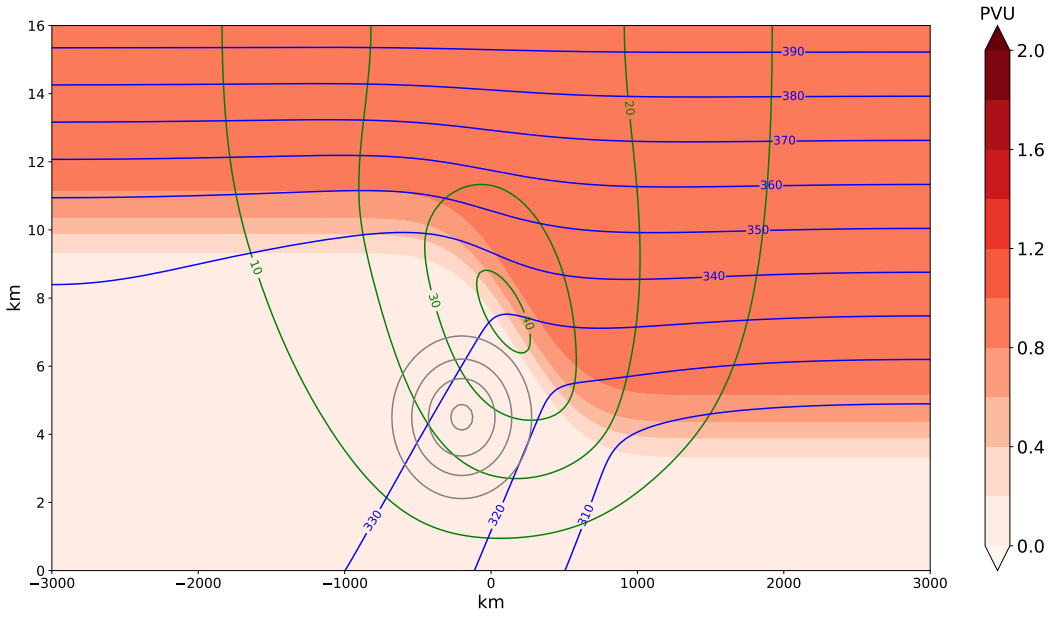

FIG. 6. **Two-dimensional frontal-geostrophic simulation setup:** Initial conditions for the two-dimensional semi-geostrophic simulation for PV (shading), zonal wind speed (green contours), potential temperature (blue contours) and diabatic heating anomaly (gray contours, from 0.1 to 0.4 $\mathrm{K\,day^{-1}}$). The horizontal axis represents the meridional coordinate.

This is expected from the formation of a negative PV anomaly (blue contour in Fig. 7) leading to anticyclonic circulation above the region of maximum heat release on the flank of the jet core and poleward advection of the tropopause by the secondary circulation induced by the heating. In contrast to reanalysis trends, which extent throughout the troposphere, the increase in zonal wind speed is confined to the area above the heating where the negative PV anomaly is formed. Assuming linearity in the response and that the jet trend is composed of an average of the responses to multiple heating events, with increasing intensity on average as climate warms, the results of the idealized frontal-geostrophic experiment suggest an intensification of the jet and slight poleward shift seen over the Gulf Stream produced by this mechanism, which is in agreement with the long-term ERA5 trend. It indicates that the mechanism has indeed sufficient amplitude to explain the trend in the jet entrance region. However, the baroclinic component of the response dominates in the frontal-geostrophic simulation in contrast to the reanalysis trend.

As outlined in the introduction, two potential mechanisms, one direct and one indirect are proposed to explain the effect of diabatic heating on the jet. The direct mechanism, which has

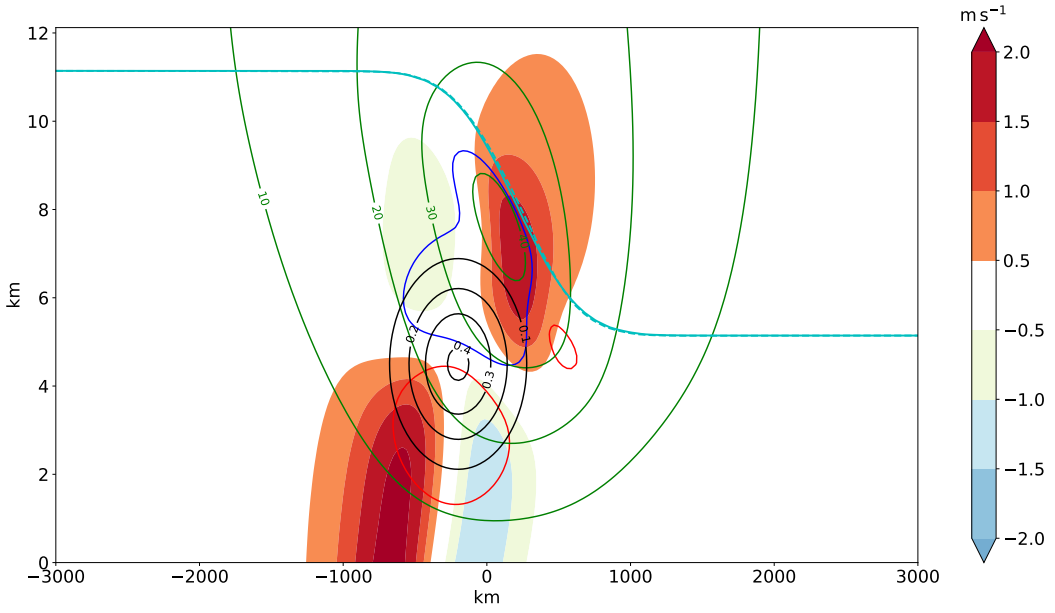

FIG. 7. **Impact of a local diabatic heating source in an idealized two-dimensional frontal-geostrophic experiment on the jet location and speed:** Shading represents the difference in zonal wind speed between final and initial states. Initial zonal wind speed is represented by green contours, diabatic heating by black lines. Red (blue) contour represents an increase (decrease) in potential vorticity of 0.025 PVU, while the light blue solid (dashed) contour indicates 0.8 PVU in the initial (final) state.

been analyzed by means of this idealized two-dimensional experiment, produces a modification of the PV via diabatic heating. This process is likely to be important at the entrance of the North Atlantic, as the heating is anchored by the land-sea contrast and the Gulf Stream SST anomaly (Minobe et al. 2008; Woollings et al. 2016). This direct mechanism is more likely to create a baroclinic structure. If diabatic heating is increased on average over many individual cyclogenesis events, a change in the mean state and an increase in the time mean baroclinicity over the Gulf Stream sector can be expected (Hoskins and Valdes 1990b; Parfitt and Czaja 2016), which is also in agreement with the enhanced baroclinicity at all levels identified in the ERA5 trends. In the indirect mechanism, diabatic heating modifies baroclinicity and consequently baroclinic growth and, finally, momentum deposit by eddies. Since baroclinic waves are typically not breaking in the western North Atlantic, the indirect mechanism is expected to become more relevant for the jet trend more downstream, despite the increase in eddy momentum convergence is found over the whole North Atlantic in midlatitudes. The increase in the mean baroclinicity will alter the

eddy-zonal flow feedback (Hoskins et al. 1983; Lorenz and Hartmann 2003), as seen by a positive trend in the E vector divergence (Fig. 5). This feedback is not limited to the Gulf Stream sector, but also affects the jet downstream into the North Atlantic, where the trend pattern indicates a push of the jet equatorward because of an increased cyclonic wave breaking tendency, indicated by the poleward E vector trend (Fig. 5b). The indirect mechanism is further explored next with idealized aquaplanet simulations.

4. Eddy-mean flow feedback

The two-dimensional frontal-geostrophic model discussed in the previous section lacks the important contribution by synoptic-scale baroclinic eddy growth and Rossby wave breaking. Therefore, in order to substantiate the changes in eddy-zonal mean flow feedback resulting from enhanced mean baroclinicity, we perform a set of simulations using a fully-fledged Atmospheric Global Circulation Model (AGCM), but in a semi-realistic configuration with typical climate model resolution. However, given the reduced complexity of these simulations, the main goal of these experiments is to identify which of the mechanisms analyzed in the reanalysis can be reproduced in this simplified and controlled setup and are therefore easier to interpret, and which ones require higher complexity or model resolution to be reproduced. The main focus is to analyze the effect of baroclinic wave eddy fluxes on the jet downstream of an imposed local SST maximum intended to mimic the land-sea contrast and the Gulf Stream and introduce a localized maximum in diabatic heating.

a. Idealized aquaplanet simulation setup

The simulations use the Icosahedral Nonhydrostatic Weather and Climate (ICON) model version 2.6.5 (Zängl et al. 2015) in an aquaplanet setup with a zonal asymmetry mimicking the land-sea contrast between North America and the Gulf Stream region. These simulations help to better understand the potential effects of change in eddy-zonal flow feedback, which is absent in the two-dimensional model. The simulations have a horizontal resolution of approximately 80 km and 70 vertical levels up to 65 km height. The physical parameterizations used include a one-moment two-category microphysics (Doms et al. 2011), Tiedke convection scheme (Tiedke 1989), a prognostic turbulent kinetic energy scheme for sub-grid turbulent transfer (Doms et al. 2011),

non-orographic gravity wave drag (Orr et al. 2010) and the ecRad radiation scheme (Hogan and Bozzo 2018).

The atmosphere initialization follows the Jablonowski-Williamson baroclinic wave test case (Jablonowski and Williamson 2006) and the SST is based on the "Qobs" distribution (Neale and Hoskins 2001) with a superposed idealized SST anomaly in the Northern Hemisphere with an amplitude of 10 K and rotated positive and negative ellipsoidal anomalies to represent the effects of both the Gulf Stream and the land-sea contrast in the North Atlantic (Fig. 8). The central point of the perturbation is located at 30°W, while three different latitudinal positions (38, 39 and 42°N are considered to analyze the sensitivity of the jet response to the position of the zonal asymmetry. Further details on the model configuration for these experiments are provided in Schemm et al. (2022).

For each experiment with different positions of the SST perturbation, two simulations are run: a control simulation with the above setup including the baseline SST distribution and the SST anomaly shown in Fig. 8 and an additional simulation that includes an SST uniform warming of 4 K on top of the setup of the control simulation. The difference between these two simulations constitutes the response to uniform warming. The SST anomaly, which represents the land-sea contrast in this idealized framework, is the same in both simulations. This constitutes an additional simplification since warming has also an impact on land-sea contrast. The response is compared to the trends identified in the reanalysis. This allows us to estimate to which degree the physical mechanisms contained in this idealized setup can explain the trends obtained in the reanalysis. The simulations are run for a period of ten years in a perpetual winter configuration. Note, however, that the trends in ERA5 contain the effects of both natural variability and anthropogenic forcing, while in the aquaplanet simulations the response reflects the impacts of the imposed warming given that the simulation period is long enough to limit the effect of internal variability.

b. Simulation results

The vertical cross section of the change in zonal wind speed, which is shown in Fig. 9a, indicates an equatorward shift at upper-levels while at lower levels the response is characterized by a slight poleward shift of the jet. Therefore, the vertical profile of the positive response in the zonal wind has a stronger meridional tilt than that detected in ERA5 (Fig. 9a). The response to uniform surface

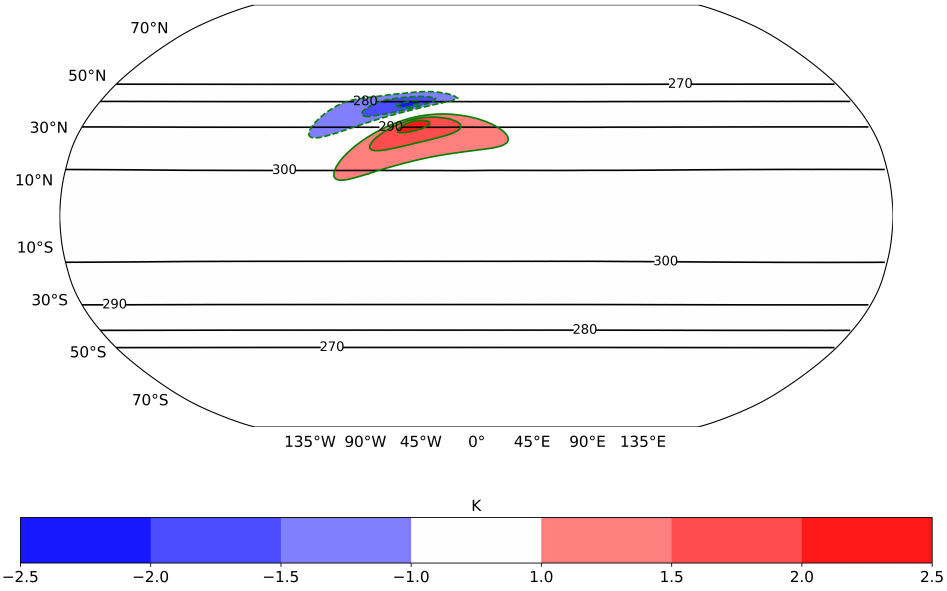

FIG. 8. **Aquaplanet simulation setup:** Setup used in the ICON aquaplanet simulations including a zonally symmetric SST profile represented by black contours from 270 to 310 K, known as "Qobs" and an SST perturbation (shading and green contours). The anomaly is centered at 30°W, 39°N.

warming by 4 K in the unperturbed Southern Hemisphere (SH) shows that in the absence of the idealized land-sea contrast, a poleward shift of the storm track is obtained (Fig. 9b), similar to what is projected by CMIP models in the SH. However, in the presence of the SST perturbation centered at 39°N, the well-marked poleward shift of the jet is suppressed (Fig. 9b,c). Instead a southwest-to-northeast oriented increase in wind speed near the SST asymmetry is observed (Fig. 9c). Further poleward, a local decrease in the wind speed is simulated (blue shading in Fig. 9c at 15°W and 70°N).

Overall, the jet response to warming resembles a southwest-to-northeast elongated pattern of enhanced wind downstream of the SST anomaly, which has a higher degree of similarity to that observed over the North Atlantic compared to a pure poleward shift seen in the SST front free SH. However, there are differences between the response in the idealized simulation and ERA5. The main contrast is that the slight poleward shift observed over the Gulf Stream is not reproduced over the SST anomaly. A possible reason why this change is not captured in these simulations is discussed in the next subsection and relates to local diabatic heating at the SST front and the findings from the two-dimensional frontal circulation model.

1) Increase in diabatic heating

The increase in diabatic heating in the warmer atmosphere has its maximum on the warmer side of the SST anomaly but downstream of its center, where baroclinic disturbances grow into mature systems as they propagate poleward (blue contour in Fig. 9b,c). Latent heat release in the accompanying warm conveyor belts in these systems is likely to contribute to the newly formed maximum in diabatic heating in this sector. Therefore, there is a mismatch in the position of the strongest increase in diabatic heating compared to ERA5 data in which the increase in diabatic heating is located more over the Gulf Stream SST front. A potential cause could be a too weak anchoring effect of diabatic heat release by the idealized SST anomaly in this fairly low-resolution simulation ($\approx$ 80 km grid spacing). For example, Sheldon et al. (2017) showed the inability to simulate the impact of the Gulf Stream on the warm sector of cyclones for a resolution of 40 km, which is twice as high than the resolution used here and in current typical climate simulations. Further studies have demonstrated that higher atmospheric and oceanic resolution leads to a local increase in diabatic heating due to enhanced vertical motion and heat and moisture fluxes over a sharper SST front (Small et al. 2014; Parfitt et al. 2017; Schemm 2023). This may explain why the increase in diabatic heating in this low-resolution simulation is greatest further downstream, where synoptic systems have grown already into mature cyclones that are better resolved by the model. Therefore, it is likely that the local response of the jet to diabatic heating, as suggested by the two-dimensional frontal simulation, which requires the meso-gamma scale to be resolved, is either not well represented or too weak.

2) Mean baroclincity and E vector change

Next, we compare the time mean baroclinicity response to warming to that found in reanalysis data. At mid- and upper levels, the change in the baroclinicity exhibits a good resemblance to the ERA5 trends (cf. Fig. 10a and Fig. 4a). The zonally averaged (30°W–45°E) cross section of the baroclinicity change depicts a tripolar pattern consisting of a positive trend at midlatitudes around the jet axis. The positive response reaches down poleward of the climatological mean jet to the 500 hPa level. The increase in slope is flanked by a reduction of the isentropic slope equator- and poleward (Fig. 10a). In the horizontal (Fig. 10b), the slope response averaged across the troposphere (250 – 850 hPa) shows a clear triple pattern, with an area of enhanced baroclinicity

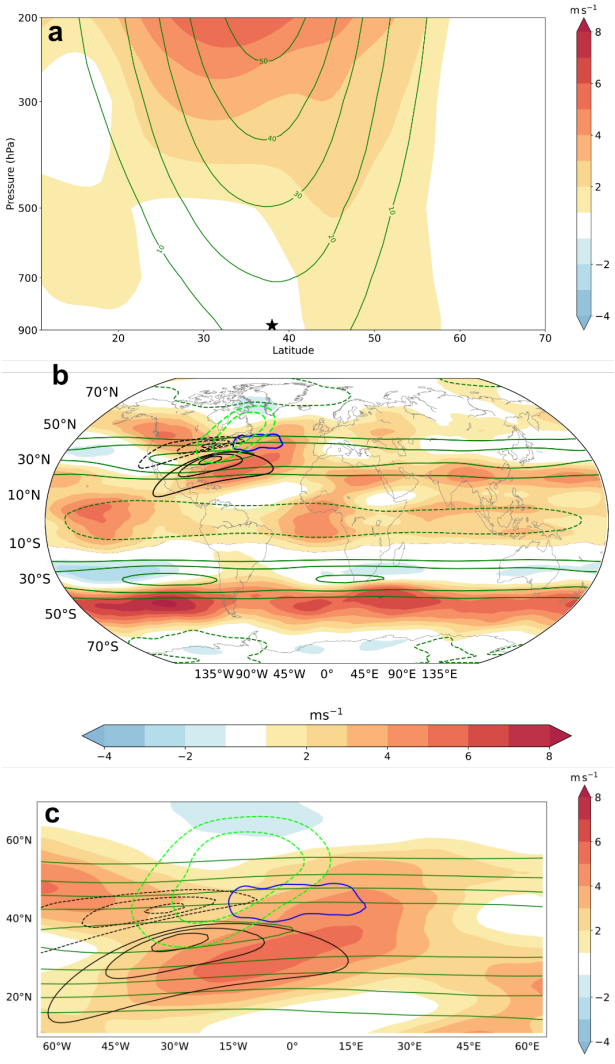

FIG. 9. **Response of zonal wind speed to uniform warming in an AGCM aquaplanet simulation:** a) Cross-section of the zonal mean zonal wind response (shading) between 30°W – 45°E in the aquaplanet simulation with a uniform warming of 4 K and the control simulation, both with an SST anomaly located at 30°W, 39°N and climatological average of the zonal mean zonal wind over the same sector in the control simulation (green contours). The black star above the x-axis indicates the latitudinal position of the SST anomaly. b) Difference between the zonal wind speed at 250 hPa (shading), climatological mean of the zonal wind speed for the control simulation (dark green contours, between 30 and 50 m s^{-1} with dashed black contour for zero zonal wind speed), diabatic heating change (blue contour, 0.4 K day^{-1}) and response in the zonal 500-hPa geopotential anomalies (light green contours at -400 and -600 m^2 s^2). The SST anomaly is represented by black contours (from -2.5 to 2.5 K). To facilitate comparison with ERA5 results (Fig. 1b), all fields in panels a and b are shifted 50° westwards. Continents are shown for illustrative purpose only. c) Zoom of the zonal wind response, climatological zonal wind, diabatic heating and geopotential anomalies into the area near and downstream of the SST anomaly.

poleward of the jet extending downstream to 45°E (red shading in Fig. 10b). Parts of this region downstream of the SST front (little star in Fig. 10b) coincide with the area of increased diabatic heating (blue contour in Fig. 9c).

The increase in time mean baroclinicity is associated with changes in eddy momentum flux as indicated by changes in the meridional component of E vectors (Fig. 11). Climatologically, the control simulation is characterized by eastward pointing E vectors at the jet axis, by poleward pointing E vectors poleward of the jet axis and by equatorward pointing E vectors equatorward of the jet axis (Fig. 11a). In agreement with theory, E vector divergence occurs at the jet core indicating eddy momentum flux convergence and acceleration (red shading in Fig. 11a). The response to warming downstream of the SST front is characterized by increased eddy momentum flux convergence in two locations (red shading in Fig. 11b). One increase is centered at 50°N (little star in Fig. 11b), and it is associated with the increase in baroclinicity (little star in Fig. 10b) and also enhanced zonal wind speed. From a mechanistic viewpoint, enhanced diabatic heat release increases the time mean baroclinicity, which strengthens the area of baroclinic wave excitation and eddy momentum flux convergence in this region. This mechanism is also found in ERA5. A second increase in eddy momentum flux convergence occurs equatorward of the mean jet position (little square in Fig. 11b). However, this increase results from the poleward shift of the wave excitation region (the main zone of baroclinicity), as it is also observed in the SH and has no associated local increase in baroclinicity (little square in Fig. 10b). In the zonal mean cross section (Fig. 11c), the change in the E vector is primarily characterised by an intensified poleward orientation, with the more equatorward-located change being connected to the poleward shift and the more poleward-located change being related to the increase in the slope.

In addition to the changes discussed above associated with the transient eddy mean flow feedback, more locally above the SST front, we find a clear increase in the stationary circulation. (light green contours in Fig. 9b,c). In this area, the response of the stationary circulation indicates the formation of a stationary trough, which appears to cause the zonal wind change locally at the front.

As already argued in the previous section, since the diabatic heating is enhanced downstream of the SST anomaly and not above its centre, the local strengthening and poleward push of the jet seen in ERA5 and in the two-dimensional frontal-geostrophic model is not reproduced. A possible cause of this discrepancy is the underresolved transient diabatic processes, which cause this local

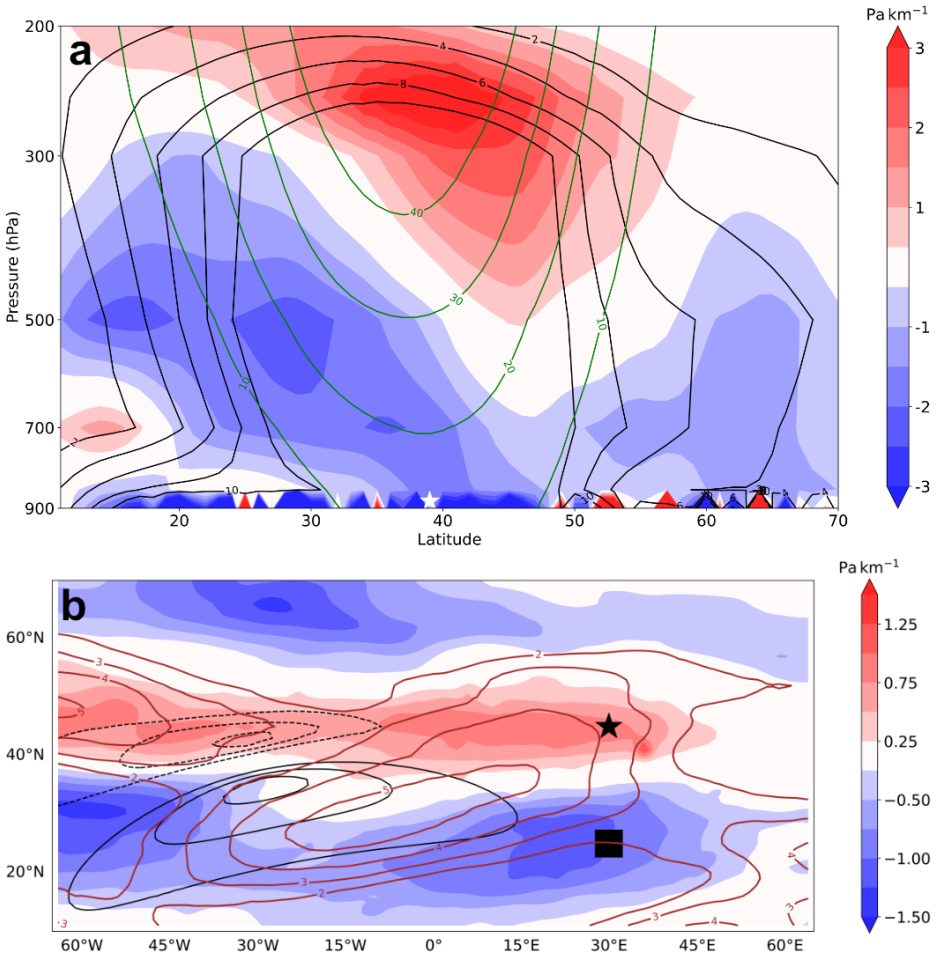

FIG. 10. **Response of isentropic slope to uniform warming in an AGCM aquaplanet simulation:** a) Cross-section of the zonal mean of the response in the slope of isentropic surfaces to a uniform warming of 4 K in the idealized aquaplanet simulations with an SST anomaly centered at 30°W, 39°N. The slope is averaged over the area between 30°W and 45°E (downstream of the SST anomaly). The climatological mean of the slope in the control simulation is represented by black contours and the zonal mean of the zonal wind speed by green contours. The white star above the x-axis represents the latitudinal position of the SST perturbation. b) Slope response to the uniform warming averaged between 250 and 850 hPa (shading) and zonal wind response at 250 hPa in the control simulation (brown contours). Black contours represent the SST anomaly. The star and the square mark regions of increased and decreased slope downstream of the SST anomaly (see text for discussion).

effect to be too weak and may be a major source of misrepresentation of the North Atlantic jet trend in low-resolution models. A thorough investigation of the effect of the model resolution on

diabatic processes is beyond the scope of this study, but diabatic heating increases at higher model resolution have recently been demonstrated in a comparable aquaplanet setup by Schemm (2023).

To summarize, the key finding of this experiment is that a zonal surface asymmetry, here an idealized representation of the land-sea contrast over the Gulf Stream sector, is sufficient to suppress the general tendency of the jet to shift poleward under warming. The response to warming of the idealized simulation includes major factors also found in reanalysis-based trends of the North Atlantic jet: increased diabatic heating near the SST anomaly, increased tropospheric baroclinicity at upper levels with a triple pattern of change throughout the troposphere at the mean storm track location, and increased convergence of eddy fluxes feeding back on the zonal flow downstream of the front causing an increase in the jet speed.

There are however some differences between this idealized run and reanalysis, namely that the positive trend in baroclinicity does not extend to the surface (Fig. 10a). Some possible causes for this mismatch could be a difference in ocean changes and air-sea exchange (Woollings et al. 2012) between the reanalysis and idealized simulations or a weaker diabatic heating within baroclinic weather systems. In addition, the idealized jet stream in the control simulation has a more zonal orientation compared to the southwest-northeast tilt identifiable in ERA5. The lack of orography in the idealized simulation could partially explain this difference in the jet orientation (Brayshaw et al. 2009). In addition, although the eddy momentum convergence coincides with the area of increased baroclinicity and stronger wind speed downstream of the SST anomaly and poleward of the mean jet position (little stars in Figs. 10b and Fig. 11b), the pattern is different from ERA5 near the SST perturbation, leading to a different jet response in this region, mainly driven by changes in the stationary circulation. There is a positive response to warming of the E vector divergence, which is not linked to a local increase in baroclinicity (little squares Figs. 10b and Fig. 11b). Furthermore, the increase in diabatic heating is located more downstream in the idealized simulation in contrast to the reanalysis, where it is more anchored over the Gulf Stream. A cause for this mismatch could be the coarse resolution of the idealized experiments. The local effect of transient diabatic heating occurring during extratropical cyclone growth over the Gulf Stream analyzed in the frontal-geostrophic simulation, which locally accelerates the jet and pushes it poleward in both the frontal-geostrophic model and ERA5, appears thus too weak to affect the mean response and thus, the changes near the SST anomaly are in contrast to the reanalysis.

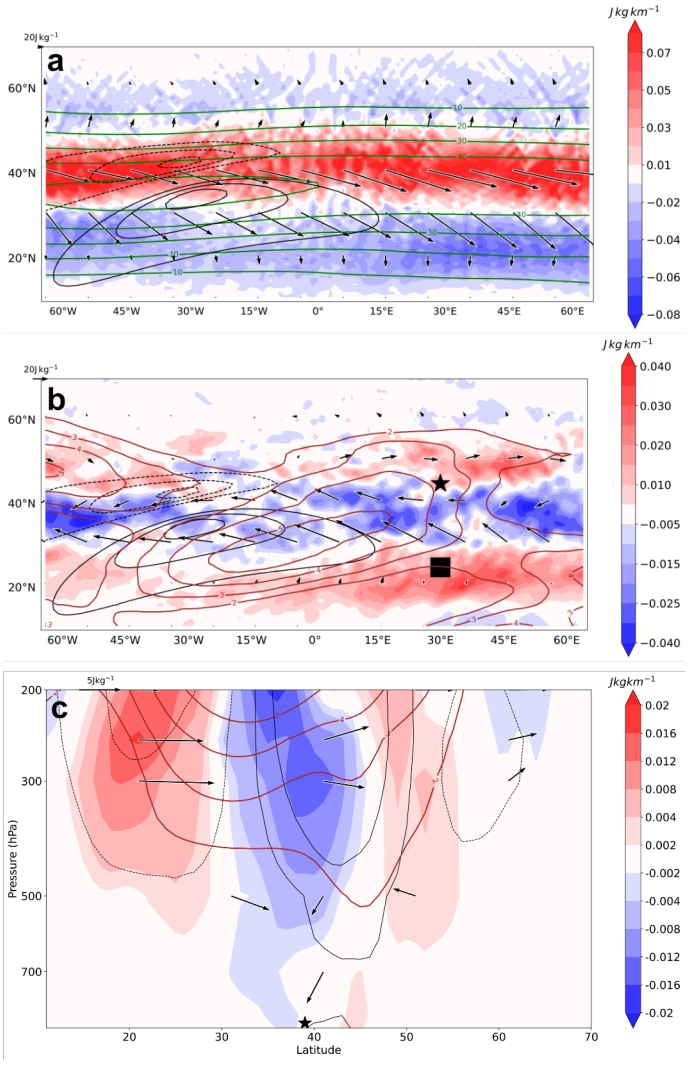

675 FIG. 11. **Response of the E vector to uniform warming in an AGCM aquaplanet simulation:** a) Clima-
676 tological mean of the E vector and its divergence (arrows and shading) in the control simulation at 250 hPa and
677 climatological mean of the zonal wind speed in the control simulation (green contours). b) Response of E vector
678 and its divergence to uniform warming at 250 hPa (arrows and shading, respectively). Brown contours depict
679 the response to warming in the zonal wind at the same pressure level. The SST anomaly is represented by black
680 contours in panels b and c. The star and the square mark regions of increased E vector divergence downstream of
681 the SST anomaly (see text for discussion). c) Cross-section of the zonal mean difference of E vector divergence
682 between warmed and control simulation (shading), climatological mean of the E vector divergence in the control
683 simulation (black contours, between -3·10^{-5} and 3 ·10^{-5} Jkg^{-1} m−1), E vector response to uniform warming
684 (arrows) and zonal wind response (brown contours) in the aquaplanet simulation with an SST perturbation located
685 at 30°W, 39°N. The black star above the x-axis indicates the latitudinal position of the SST perturbation.

3) Sensitivity to the position of the SST anomaly

The purpose of the next simulations is to change the exact location of the convergence of the upper-level eddy momentum flux and increase in diabatic heating relative to the mean jet position. This is done by changing the location of the SST anomaly (to 38 and 42°N) relative to the mean jet position, which is set by the large-scale SST gradients according to the Qobs SST distribution.

The response of the storm track to warming downstream of the SST anomaly (east of 0°) in both simulations is characterized by an increase of the zonal wind speed poleward of the climatological jet position (Fig. 12). Both simulations feature a triple pattern in the baroclinicity response (Fig. 13a,b), which is more confined in the upper levels and is also slightly displaced towards the equator in the simulation with the SST front at 38°N (Fig. 13c). In both simulations, the increase in diabatic heating is located downstream of the idealized land-sea contrast (not shown), in line with the simulation with an SST front at 39°N (Fig. 9b,c). In this downstream area (little star in Fig. 13c,d), the response is dominated by an increase in baroclinicity and a corresponding intensification of eddy momentum flux convergence. This behavior is independent of the position of the SST asymmetry.

Conversely, the response near the SST anomaly differs between the two front positions. In the case of a more equatorward SST anomaly, the jet shifts equatorwards (Fig. 12a) and the difference between the warmed and control simulations features poleward pointing E vectors and a positive difference in E vector convergence over the storm track entry region equatorwards of the mean jet position (Fig 13c), which pushes the jet equatorward. In the other sensitivity simulation with a more poleward located SST anomaly, the jet clearly shifts poleward near the SST front and up- and downstream of it (Fig. 12b), similarly to what occurs in the absence of the SST anomaly in the SH (Fig. 9b). Accordingly, slope and eddy momentum convergence also shift polewards under warming (Fig. 13b,d) and the increase in the isentropic slope is much less confined to upper levels.

In the unperturbed SH there is also some variability between different simulations (not shown), but the response is qualitatively similar featuring a poleward shift in all simulations, in contrast to the NH where the position of the SST anomaly has a higher impact on the jet response than the variability detected in the SH.

The three experiments with different positions of the SST anomaly show that if this perturbation is located near the mean jet position the response to uniform is not a poleward shift as it occurs

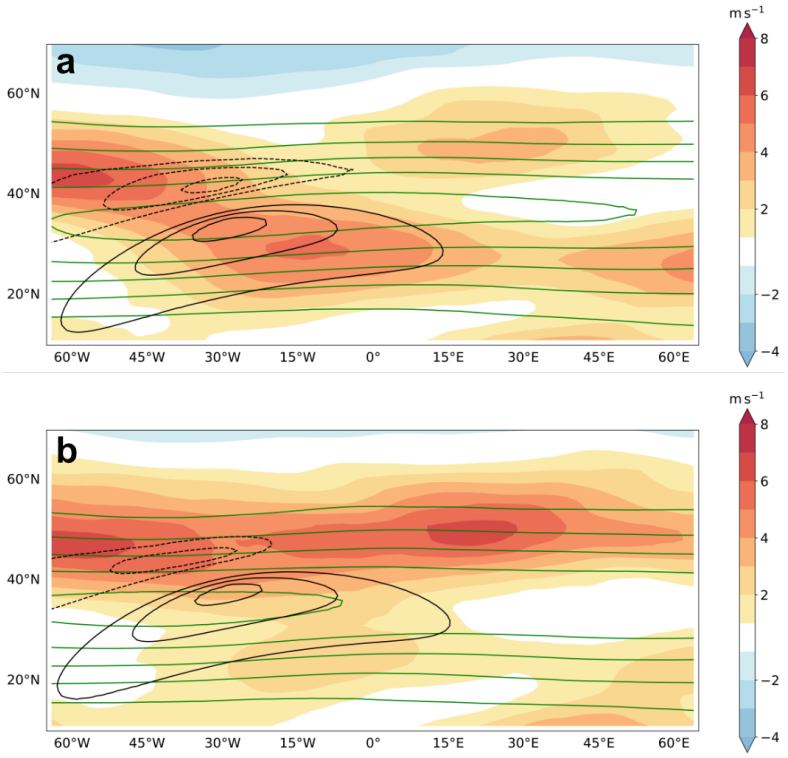

751 FIG. 12. **Sensitivity of the zonal wind response to the position of the SST anomaly in aquaplanet**
752 **simulations:** Difference between the zonal wind speed in the aquaplanet simulations with a uniform warming
753 of 4 K and the control simulation at 250 hPa (shading), and climatological zonal wind speed in the control
754 simulation (green contours between 30 and 50 ms^{-1}) with an SST anomaly located at 30° W, a) 38°N and b)
755 42°N. Black contours represent the SST perturbation.

744 when there is no anomaly or when it is located far from the mean jet position. The role of changes in
745 stationary circulation for the wind response near the anomaly is strongly dependent on its position
746 as shown in the experiments with the SST perturbation at 38°N, where the stationary circulation has
747 a limited influence, and the simulation with the SST anomaly at 39°N, where the response in this
748 sector is dominated by changes in the stationary circulation. Downstream of the SST asymmetry,
749 the response in all simulations is dominated by an increase in diabatic heating, which enhances
750 baroclinicity and eddy momentum convergence poleward of the mean jet position.

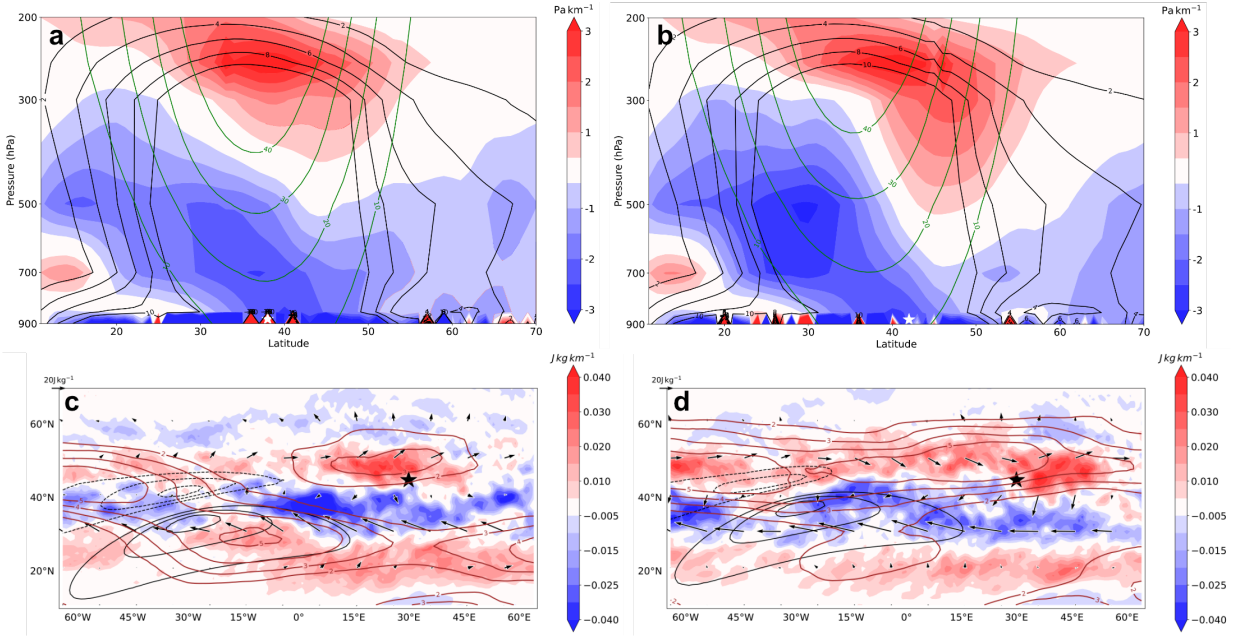

FIG. 13. **Sensitivity of the baroclinicity and E vector response to the position of the SST anomaly in aquaplanet simulations:** Cross-section of the response of the slope of the isentropic surfaces under global warming (shading) and climatological mean of slope and zonal wind in control simulations (black and green contours, respectively) with an SST anomaly located at 30° W, a) 38°N and b) 42°N. White stars above the x-axis in panels a and b represent the latitudinal position of the SST anomaly. c), d) Response of the E vector and its divergence (arrows and shading, respectively) at 250 hPa for both sensitivity experiments and response in the zonal wind at the same pressure level (brown contours). The SST anomaly is represented by black contours in panels c and d. The stars in panels c and d mark a region of increased E vector divergence downstream of the SST anomaly (see text for discussion).

5. Fully-coupled CESM ensemble simulations with SSP3-7.0 scenario

Finally, we examine the extent to which the trends identified in the reanalysis are reproduced by a historical run of fully-coupled climate model over the ERA5 period. It has been recognized that the current generation of fully-coupled Earth system models appears to be missing the trend in the North Atlantic jet stream (Blackport and Fyfe 2022). Here, we examine zonal wind and baroclinicity trends in an ensemble of fully-coupled climate simulations.

a. CESM model setup

The ensemble consists of 5 climate simulations produced with the Community Earth System Model (CESM) version 2.1.2 (Danabasoglu et al. 2020), labeled 0900 to 1300. These are used to compare the ERA5 trends with simulated historical trends and to analyze future projections for the jet stream. The model is run in fully coupled mode including the Community Atmosphere Model (CAM6) (Bogenschutz et al. 2018; Danabasoglu et al. 2020) with 32 vertical levels, the Community Land Model (CLM5) (Lawrence et al. 2019), the Parallel Ocean Program version 2 (POP2, 60 vertical levels), the Los Alamos National Laboratory Sea Ice model (CICE5) (Hunke et al. 2015), and the hydrological routing model Model for Scale Adaptive River Transport (MOSART) (Li et al. 2013). The horizontal resolution is approximately 1°. The historical period with prescribed forcing covers from 1850 to 2014, and from 2015 to 2100 the runs are forced with the SSP3-7.0 scenario, which constitutes a medium to high forcing pathway (O'Neill et al. 2016). To provide a more meaningful comparison with the ERA5 data, the period 1980-2022, which is partially driven by the SSP3-7.0 forcing, is used as the historical period.

b. Historical period (1980–2022):

The ensemble mean trend for the historical period (1980–2022) displays a well-marked equatorward shift of the jet over the Gulf Stream region and downstream extension (Fig. 14a), which is different from the local poleward shift identified in the reanalysis over the Gulf Stream sector. A closer inspection of the ensemble mean of the slope trend shows that also the increase in the baroclinicity is located equatorwards with respect to the jet position (between 25–40°N, Fig. 14b). Considering the role of the local increase in transient diabatic heating in pushing the jet slightly poleward, this effect seems to be either absent or not strong enough to result in a local increase and poleward displacement of the jet stream. Nevertheless, some caution is required to interpret these differences as model error given the small ensemble size, which may not be sufficient to isolate the forced response. In addition, reanalysis trends as presented in section 2 are the result of a combination of external forcing and natural variability, which is particularly large in the historical period as seen in the CESM ensemble spread. Appendix B further illustrates this aspect by analyzing daily zonal wind data for a subset of 50 members of the CESM2 large ensemble (CESM-LENS) (Rodgers et al. 2021).

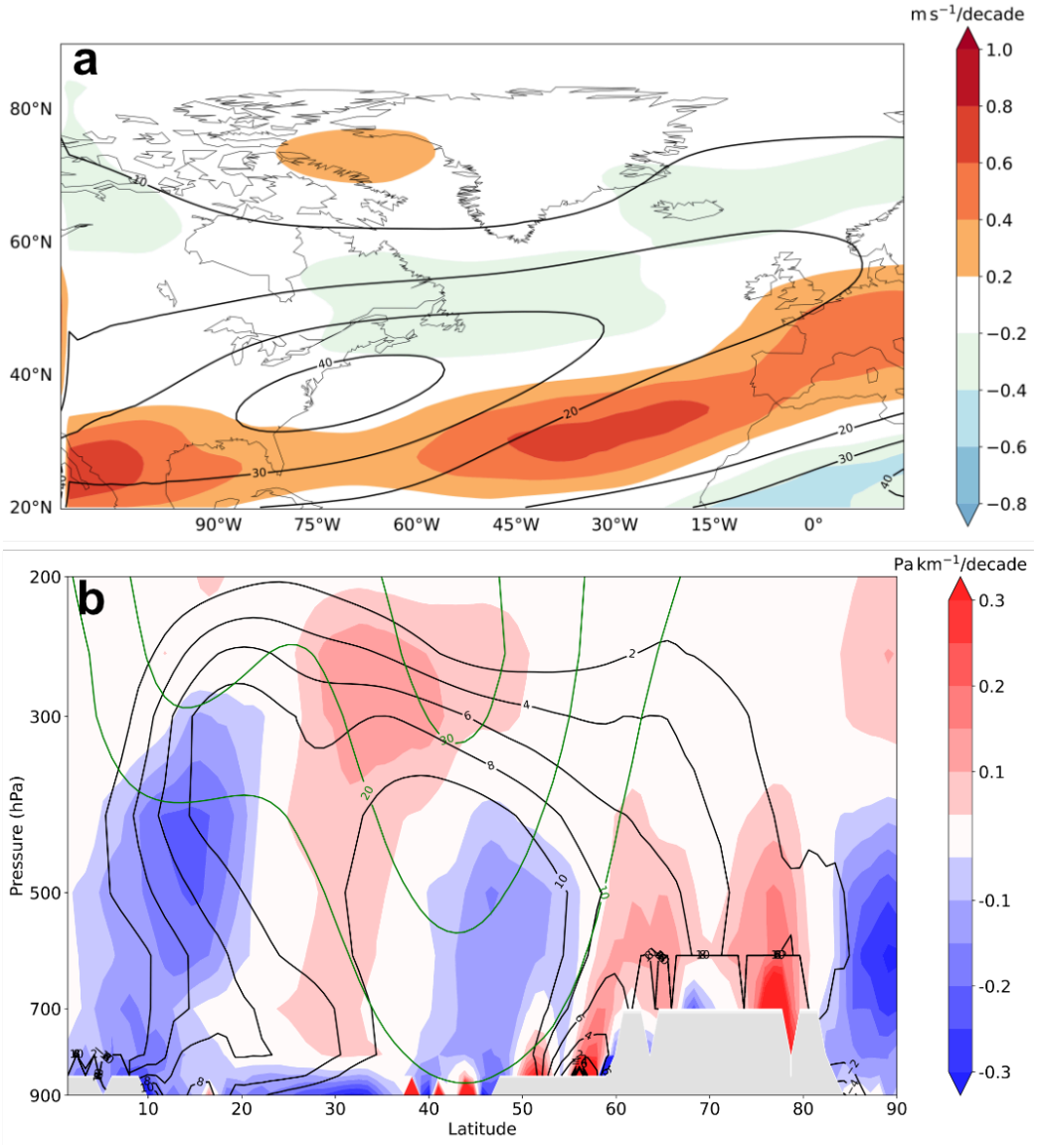

FIG. 14. **DJF trends in 250-hPa zonal wind speed and in a vertical cross-section of the slope of the isentropic surfaces for CESM simulations in the historical period (1980-2022):** a) Trend in zonal wind speed (shading) and climatological mean (black contours) for the historical period. b) Trend in the slope of the isentropic surfaces (shading) and climatological mean (black contours) over the North Atlantic storm track (80–15° W). Zonal wind speed climatology is represented by green contours.

However, the ensemble spread of wind speed trends in the CESM ensemble simulation in the historical period is remarkably large, as is the direction of the meridional shift of the jet among the different ensemble members (Fig. 15). This diversity is aligned with different responses of

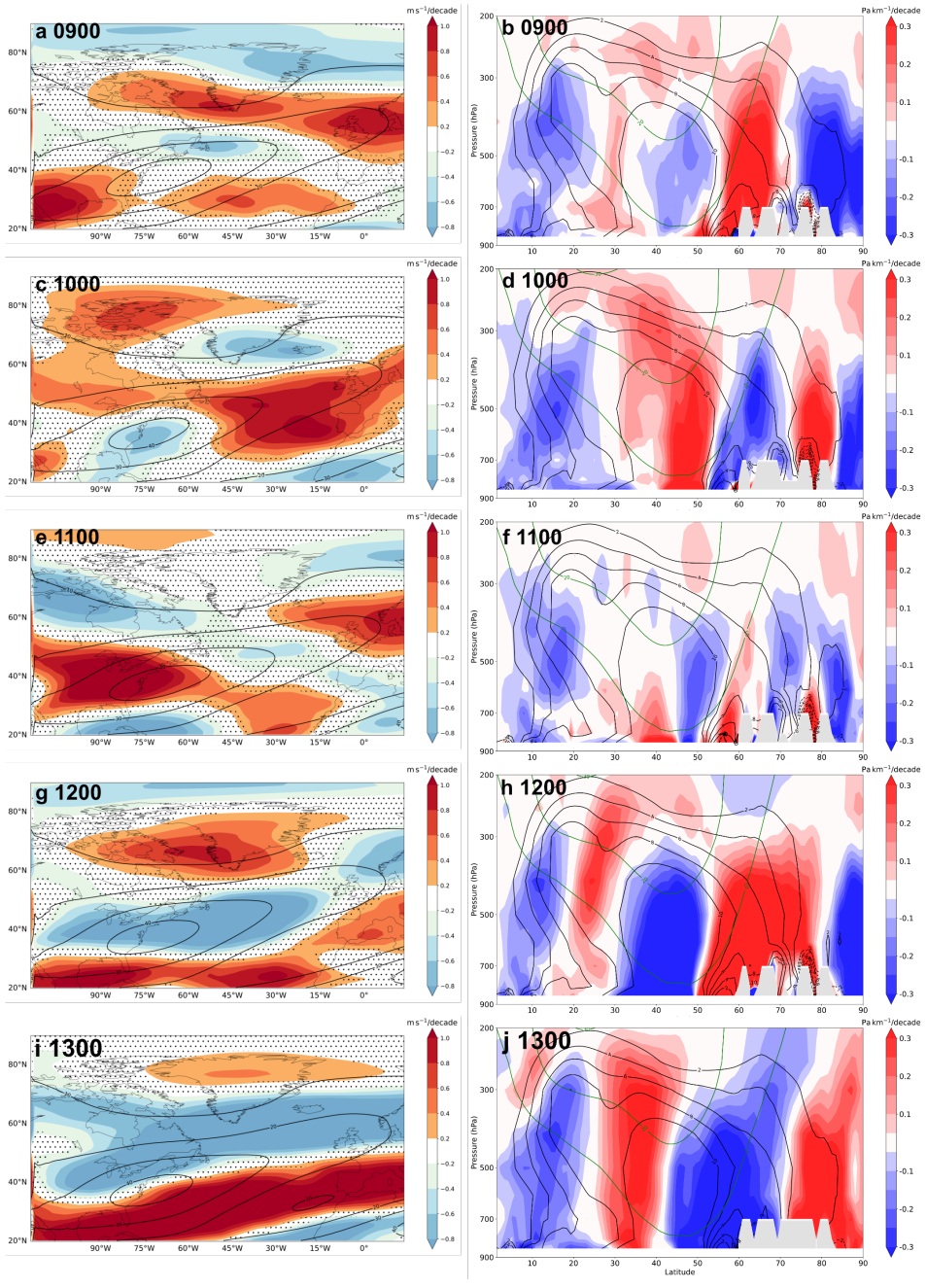

805 FIG. 15. **DJF trends in 250-hPa zonal wind speed and in a vertical cross-section of the slope of the**
806 **isentropic surfaces for each CESM ensemble member in the historical period (1980-2022):** As in Fig. 14
807 for each ensemble member.

811 the baroclinicity to warming across the ensemble, similarly to the effect of shifting the position of
812 the SST anomaly in the aquaplanet simulations. In particular, there are differences in the exact

position of the positive baroclinicity trend relative to the climatological mean, which is essential in determining the jet shift (Yuval and Kaspi 2016). For example, member 0900 displays a poleward shift with a positive zonal wind trend around 60°N, which is accompanied by a positive slope in trend in the same region (Fig. 15a,b). Conversely, member 1300 displays a tripolar pattern of change (Fig. 15j) as expected from zonal asymmetries (Schemm et al. 2022). However, the positive slope trend is also for this member located slightly equatorward of the mean jet position and consequently the positive wind trend is displaced to the south (Fig. 15i), similar to the ensemble mean (Fig. 14). The remaining members exhibit larger differences some members produce a poleward shifted positive baroclinicity trend but no downstream extension, while some do not reproduce the tripolar pattern in the slope trend at all. At upper levels, all members exhibit a negative trend in stability due to either stratospheric cooling or reduced warming in midlatitudes, which results in an overall positive slope trend, but there is widespread disagreement on the location of the positive slope trend.

As a consequence of the large ensemble spread, the ensemble mean trend in momentum convergence is close to zero as opposing trends in individual ensemble members cancel each other (not shown). While the closest member to ERA5 shows a significant increase in the northward component of the E vector, other members produce lower increases or even an equatorward pointing trend.

c. End of century (2057–2100)

The ensemble mean of the trends for the end of the century remains fairly similar to that of the historical period but is amplified (Fig. 16a). Again, baroclinicity features a notable increase equatorward of the mean jet position between 25–35°N throughout the troposphere and a negative trend between 40–50°N at mid- and low levels (Fig. 16b), which indicates that the exact location of the modeled positive trend in baroclinicity is a potential source of uncertainty in future projections.

Differences in the ensemble spread are now reduced compared to the historical period. At the end of the century, all ensemble members project an equatorward shift of the jet which is well reflected in the ensemble mean (Fig. 16b). Contrary to what is found for the historical period, now all members produce a positive slope trend around or equatorward of the mean jet position at low levels (Fig. 17b) but 10° too equatorward compared to observed recent trends. This is associated

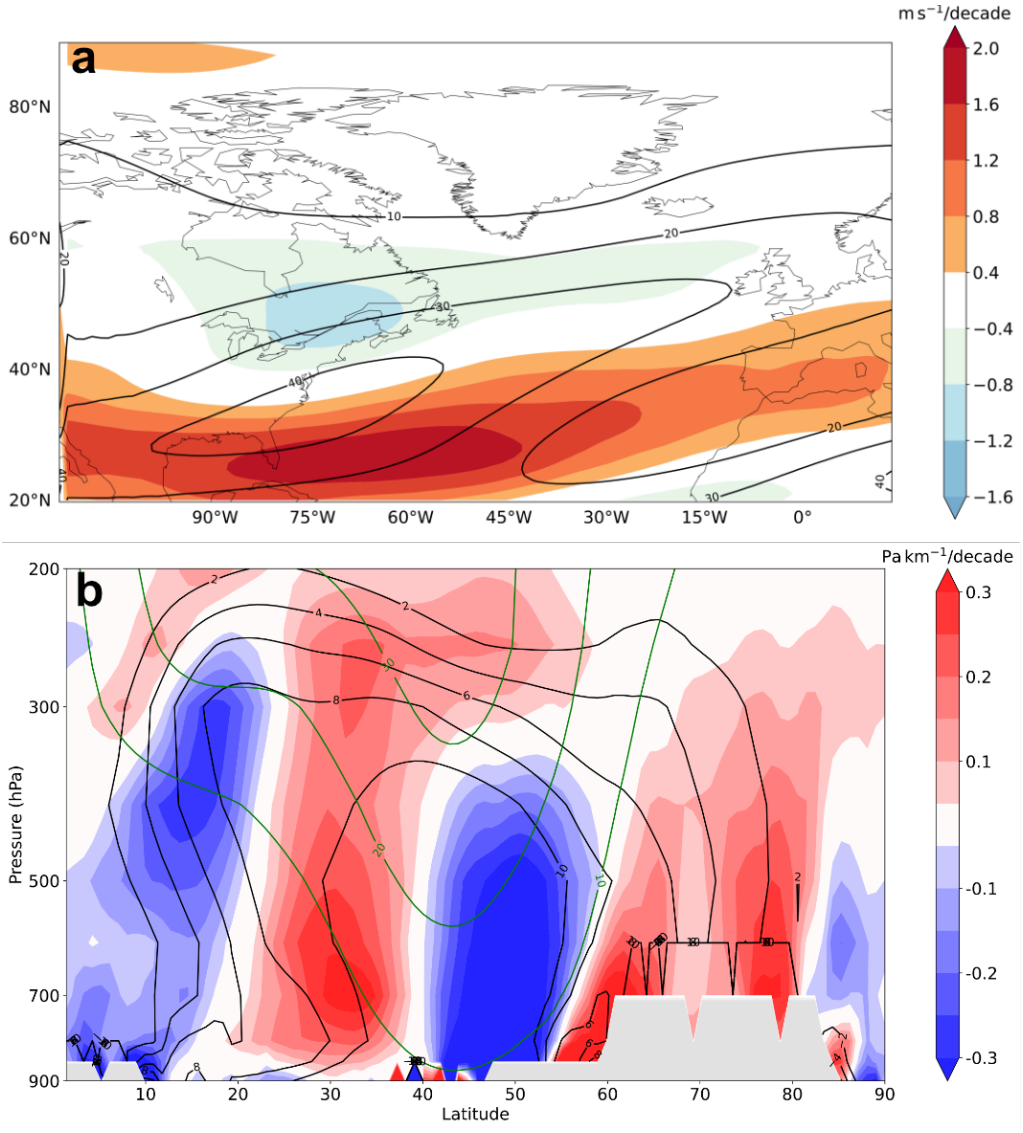

FIG. 16. **Trends in 250-hPa zonal wind speed and in a vertical cross-section of the slope of the isentropic surfaces for CESM simulations in the end of the century period (2057-2100):** As in Fig. 14 for the end of the century period. Note the different color scale for the wind trend compared to Fig. 14.

with a small warming trend at midlatitudes, which increases the meridional potential temperature gradient and thus, the slope. At upper levels, the pattern is similar to the one obtained for the historical period. In general, all members display a well-marked equatorward shift (Fig. 16a), similar to the aquaplanet simulation with zonal SST anomalies centered at 39°N. Further, the triple pattern in the slope and potential temperature trends emerges (Fig. 16b). Therefore, the baroclinicity and the jet trend seem both placed too far to the equator compared to recent trends in

ERA5. The reduced ensemble spread at the end of the century and the large spread in the more recent period indicate a small signal to noise ratio in the historical period, while it is stronger at the end of the century, as a consequence of intensified warming in this period (Rodgers et al. 2021).

Overall, we find that the results over the Gulf Stream sector for the 5-member ensemble are different from the reanalysis with an equatorward shift in the ensemble mean of the CESM simulations, and a slightly poleward shift in ERA5. The downstream extension is found in both reanalysis and CESM ensemble simulations, but the extension affects the Iberian peninsula in CESM while it affects the UK in reanalysis data, due to the equatorward shift projected for the entire North Atlantic in the climate simulations. Also the triple pattern of change is found in vertical cross sections of changes in the isentropic slope, but again shifted towards the equator in CESM. This mismatch is reduced when consideration is given to the CESM-LENS in the historical period, where some members indeed feature a polewards shift as seen in ERA5, while the majority of members still feature an equatorward shift (see Appendix B).

The signal for the end of the century consists of an equatorward shift over the Gulf Stream and an extension of the jet towards southwestern Europe. As shown by the results of the idealized two-dimensional frontal-geostrophic experiment, an increase in diabatic heating over the Gulf Stream region leads to a slight poleward shift of the jet. Therefore, it remains an open question whether the trend for the end of the century detected in the CESM climate simulations is the actual response to the increase in greenhouse gases or it is the result of a misrepresentation of the local effect of diabatic heating over the Gulf Stream. A more detailed analysis using a large ensemble as well as higher resolution simulations, such as those produced by HighResMIP Haarsma et al. (2016), is required to prove this aspect. Given the coarse resolution at which both the aquaplanet and the fully-coupled climate simulations are run, this aspect could have an impact on the trends over the Gulf Stream following the resolution argument of Sheldon et al. (2017). More research on the role of model resolution in setting the jet response to warming is needed to quantify its effect on the jet stream trends.

6. Conclusions

Atmospheric dynamics play an important role in the development of the North Atlantic jet stream and storm tracks. In this study, two main mechanisms are outlined to better understand

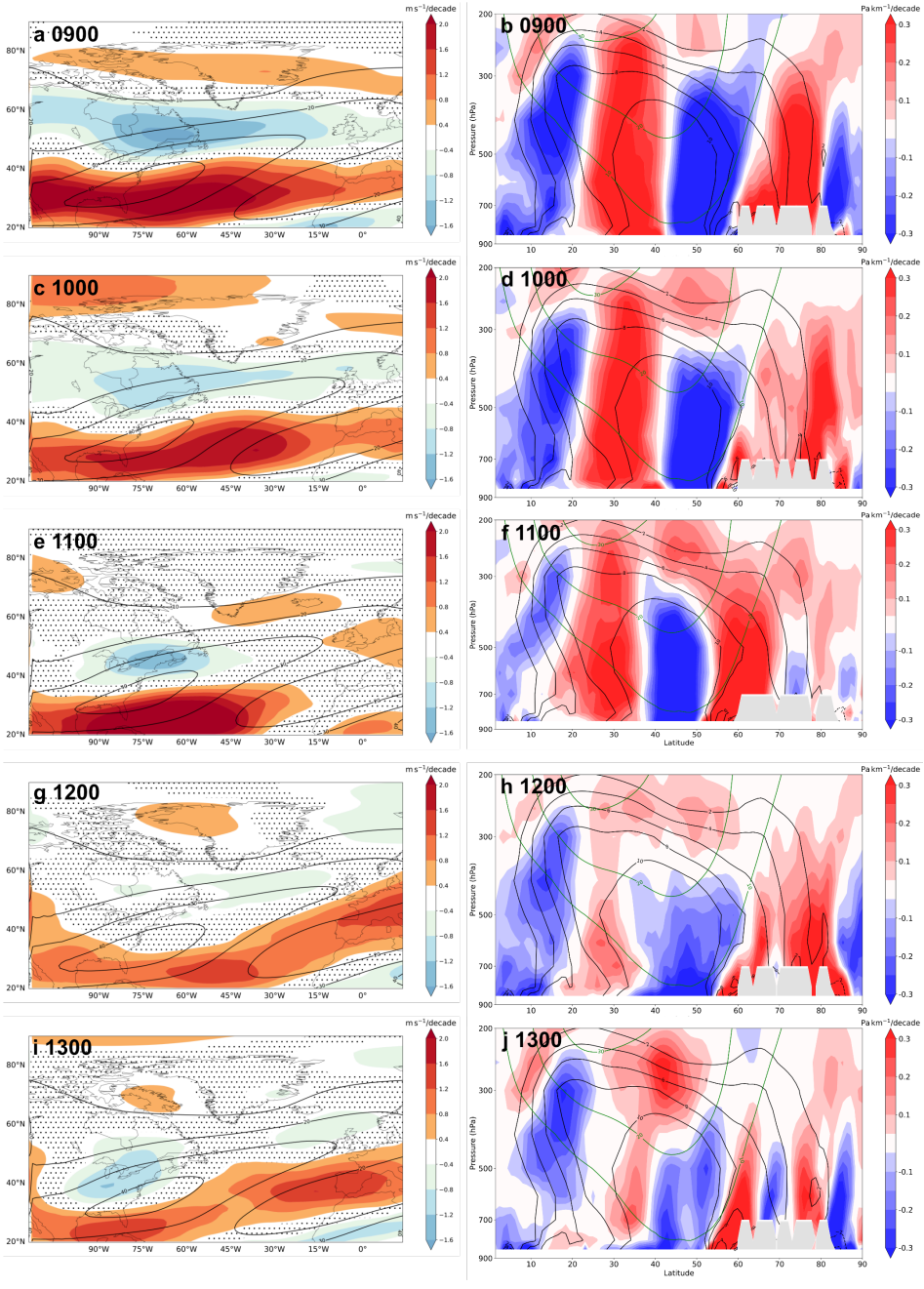

FIG. 17. **Trends in 250-hPa zonal wind speed and in a vertical cross-section of the slope of the isentropic surfaces for each CESM ensemble member in the end of the century period (2057-2100):** As in Fig. 15 for the end of the century period. Note the different color scale for wind trends.

trends in the position and strength of the North Atlantic jet found in reanalysis data. At the heart of both is the effect of enhanced diabatic heating, which (i) produces a local transient negative PV

anomaly at upper levels (Wernli and Davies 1997; Pomroy and Thorpe 2000), and (ii) increases the baroclinicity in the storm track entrance region at the core of the mean jet, which results in enhanced eddy momentum fluxes downstream (Hoskins et al. 1983; Vallis 2017). We explore each of these mechanisms with different diagnostics and modeling approach in the spirit of Peng and Whitaker (1999) by analyzing the ERA5 reanalysis and a hierarchy of model simulations with different complexity including a two-dimensional frontal-geostrophic simulation, aquaplanet experiments with an atmospheric global circulation model and fully-coupled climate simulations.

Locally, over the Gulf Stream region, where synoptic waves grow but yet do not break, an intensification and poleward shift of the jet is consistent with the response to more intense transient diabatic heating pulses during the growth and rapid succession of growing baroclinic waves (mechanism i). The response predicted by a frontal-geostrophic model forced with a heating anomaly inspired in the long-term trend observed in ERA5 is sufficient to explain the magnitude of the jet change seen in reanalysis data. However, this effect seems to be absent (or too weak) in the aquaplanet, but also in the ensemble of CESM climate simulations. A potential cause is related to the coarse model resolution and a too weak representation of the local diabatic effect and possibly is one cause of the failure of climate model to capture the North Atlantic jet response to warming as highlighted by Blackport and Fyfe (2022). Further analysis with larger ensembles and higher resolution runs, for instance HighResMIP simulations (Haarsma et al. 2016) is required to quantify the impact of model resolution on this mechanism.

Downstream of the Gulf Stream sector, the jet is further modified in ERA5 through an eddy feedback, which is consistent with an increase in baroclinicity through diabatic heating (mechanism ii) and intensified propagating Rossby waves away from the main wave source (Vallis 2017). This mechanism affects the jet over the whole North Atlantic in contrast to the local effect over the Gulf Stream produced by more intense diabatic heating pulses. The concomitant meridional propagation of Rossby waves away from the main wave source is followed by a strengthening of the eddy momentum convergence resulting in an intensification and zonal extension of the jet. The mechanism is demonstrated through analysis of changes in E vectors in idealized aquaplanet warming simulations in the presence of an SST front. The chain of mechanisms consists of increased diabatic heating slightly downstream of the SST front, intensified mean baroclinicity and enhanced eddy momentum convergence leading to an increase of the wind speed downstream of

the front. The mechanism seems to be rather independent of the exact position of the SST front. However, the jet response at the location of the SST front is strongly influenced by the position of the front and varies from a local poleward to an equatorward jet shift depending on the exact position of the SST front. For the latter case, the formation of a stationary trough over the front is a relevant factor in explaining the shift in the aquaplanet experiments.

The different methods considered here aim to foster a mechanistic understanding of the jet response, primarily to increased diabatic heating. They could also help to explain the failure of coarse climate models to simulate the recent trends in the North Atlantic (Blackport and Fyfe 2022). In our experiments, the 5-member ensemble of fully-coupled model in particular failed to simulate the local poleward shift over the Gulf Stream region observed in ERA5. A larger ensemble size is required to capture the observed trend within the ensemble spread, as can be seen in the CESM-LENS (Rodgers et al. 2021). The idealized aquaplanet simulations are unable to adequately represent the jet trend near the zonal asymmetry, which is intended to mimic the effects of land-sea contrast and the Gulf Stream. This is, as indicated above, possibly due to underrepresentation of the local effect of diabatic heat pulses, which has the potential to shift the North Atlantic poleward and strengthen it. This goes hand-in-hand with a coarse resolution in the SST fields (Sheldon et al. 2017), which strongly affects the location of enhanced baroclinicity and diabatic heating. In the previously cited study, a well-resolved SST anomaly above the Gulf Stream is shown to anchor the diabatic heating more consistently above its warm side and km-scale models have been shown to increase the magnitude of the diabatic heating over the SST anomaly (Schemm 2023). The implication from our study is that a better anchoring and increased amplitude of local transient heating is in general able to push the jet poleward. The coarse idealized aquaplanet simulations reproduce some of the main aspects of the mechanisms previously outlined, namely increased tropospheric baroclinicity at upper levels, and increased convergence of eddy momentum flux associated with Rossby wave propagation downstream of the zonal SST asymmetry, but the experiments also miss the local jet response directly above the SST front. Thus, the anchoring effect and influence of local diabatic heating pulses are likely too weak and the area of increased diabatic heating is moved downstream of the main cyclogenesis region pinpointing again to too coarse model resolution.

The analysis performed here provides a dynamical interpretation of the trends detected in the reanalysis, but an attribution to either anthropogenic forcing or natural variability has not been conducted. There are multiple dynamical adjustment methods that aim to disentangle the forced response of a magnitude of interest, usually temperature or precipitation, from natural variability. These techniques have shown satisfactory results in previous studies (Smoliak et al. 2015; Lehner et al. 2017; Guo et al. 2019; Sippel et al. 2019; Heinze-Deml et al. 2021). A foreseen study will aim at adapting this technique to the North Atlantic jet stream trends to investigate which changes are attributable to anthropogenic climate change.

Acknowledgments. This work was supported by the Swiss National Science Foundation through project grant Nr. 204181.

Data availability statement. The ERA5 data are publicly available on the Copernicus Climate Change Service (C3S) Climate Data Store: `https://doi.org/10.24381/cds.adbb2d47` (Hersbach et al. 2023). ICON simulations used for this paper will be archived at ETH Zurich's Research Collection for scientific publications and research data under a CC-BY 4.0 license for at least the upcoming 15 years (doi will be provided after acceptance). ETH Zurich's Research Collection adheres to the FAIR principles. CESM simulation data will be stored at the Institute of Atmospheric and Climate Science, ETH Zurich, for at least 10 years and will be available on request.

APPENDIX A

Zonal wind trends in ERA in the period 1940-1978

Wintertime trends in ERA5 before the satellite era (1940-1978) show an equatorward shift of the jet in the Gulf Stream region with a defined southwest-northeast orientation (Fig. A1). This contrasts with the trend for the more recent period, which is mainly characterized by a slight poleward shift of the jet over this region (Fig. 1). Downstream over central and eastern North Atlantic there is a strong intensification, an equatorward shift and an extension of the jet affecting southwestern Europe. The trend shows a decrease of zonal wind speed over the Hudson Bay and between Iceland and the British Isles and some areas at low latitudes, but there is no clear triple pattern in the trends for this period. In addition, there is a clear positive trend at high latitudes, in contrast to the later period shown in Fig. 1. The significant trends are mainly located over the ocean, where the reanalysis might not be well constraint in this period given the scarcity of observations in the considered period.

APPENDIX B

Zonal wind trends in the CESM2 large ensemble (CESM-LENS)

The ensemble mean of the selected members of the CESM2 large ensemble (CESM-LENS) for the period 1980-2022 shows a poleward shift of the jet over the North Atlantic (Fig. B1a),

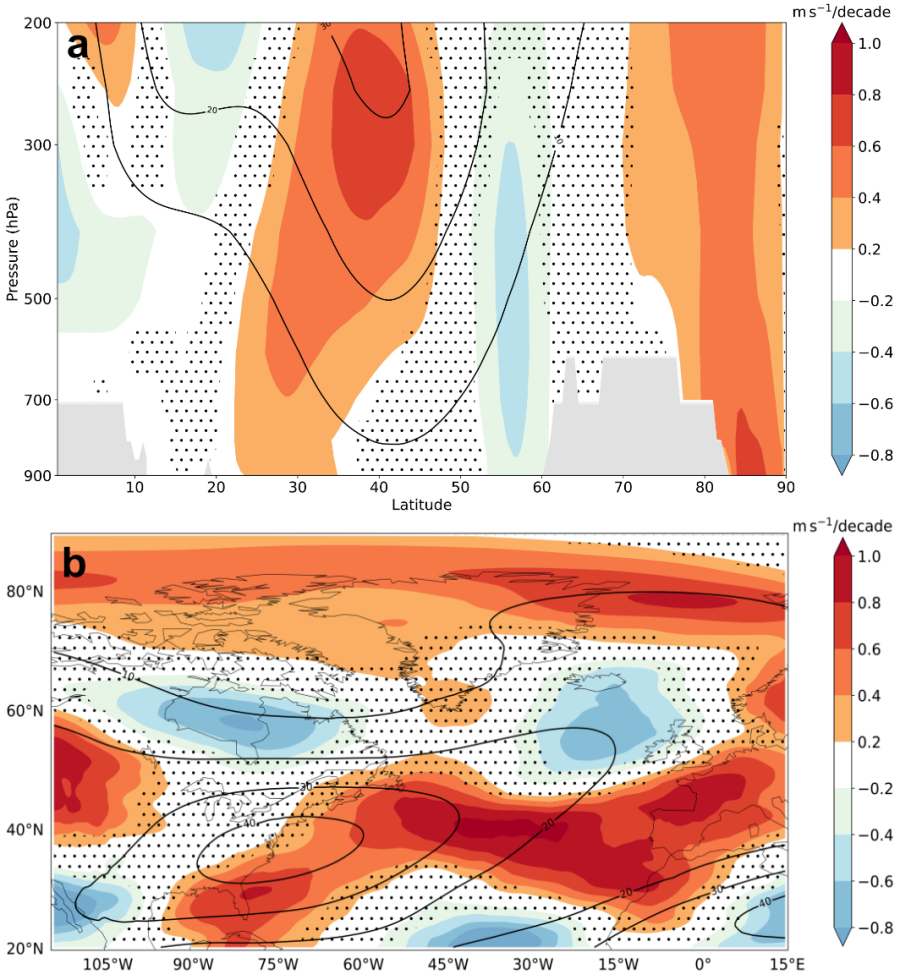

FIG. A1. **Wintertime zonal wind speed trend over the North Atlantic in ERA5 (1940-1978):** a) Mean of the trend (shading) and climatological average in zonal wind speed (black contours) over the North Atlantic storm track region (80°W – 15°W) for DJF in the period 1940-1978. b) Zonal wind trend (shading) and climatological mean (black contours) at 250 hPa. The stippling represents areas with p-values higher than p^* (see text for details).

in contrast to the small ensemble analyzed in section 5. However, the ensemble spread for the CESM-LENS is also remarkably large in this period with some members showing a poleward shift and others an equatorward shift as can be identified in the ensemble spread, which exhibits two areas of high spread equatorward and poleward of the mean jet (Fig. B1c). However, the trend displayed by ERA5 in mid and low latitudes is well captured by some ensemble members and contained within the distribution of the CESM-LENS (Fig. B2).

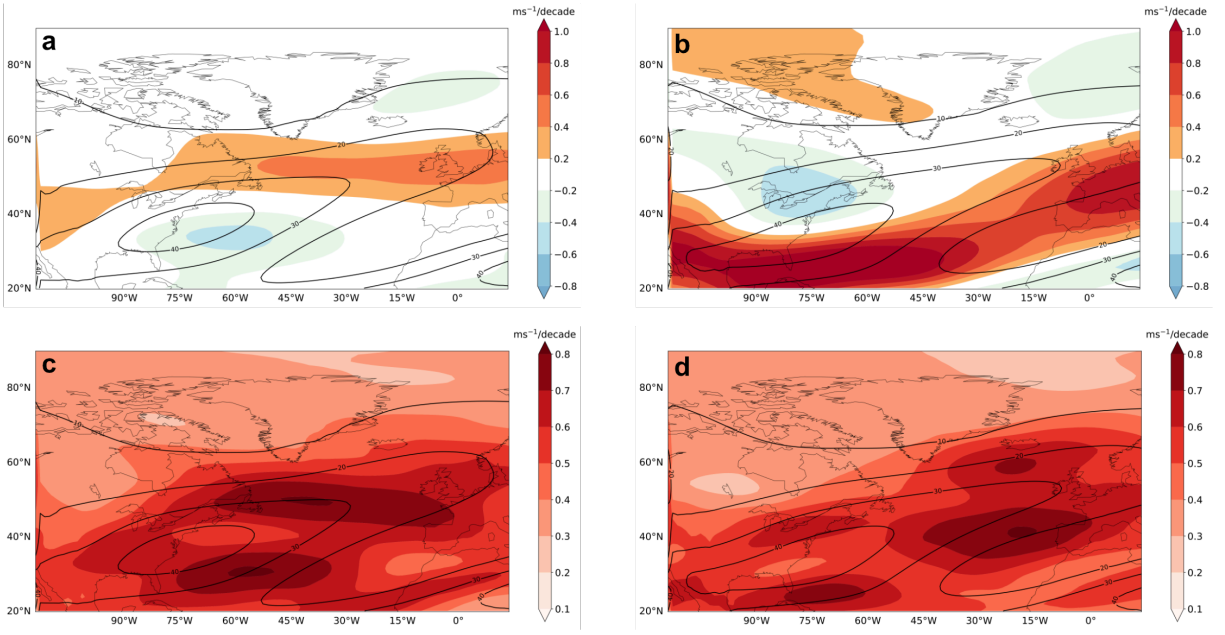

FIG. B1. **Mean and spread in zonal wind speed trends for the CESM-LENS**: Mean trend in zonal wind speed (shading) and climatological mean (black contours) for a) the historical period (1980-2022) and b) the end of the century period (2057-2100) at 250 hPa. c), d) Standard deviation of the trend in zonal wind speed (shading) and climatological mean of the zonal wind speed (black contours) for both periods at the same pressure level.

An inspection of the ensemble mean and spread for the end of the century period (2057-2100) in the CESM-LENS shows a larger signal to noise ratio in this period (Fig. B1b,d) with most of the members showing positive trends equatorward of the mean jet over the Gulf Stream and an extension over Europe. However, there is still some variability in the position of the extension over Europe and the strength of the positive trend as it is depicted by both the 5-member ensemble and the CESM-LENS (Figs. 17 and B1d).

References

Ambaum, M. H. P., and L. Novak, 2014: A nonlinear oscillator describing storm track variability. *Quarterly Journal of the Royal Meteorological Society*, **140**, 2680–2684, https://doi.org/10.1002/qj.2352.

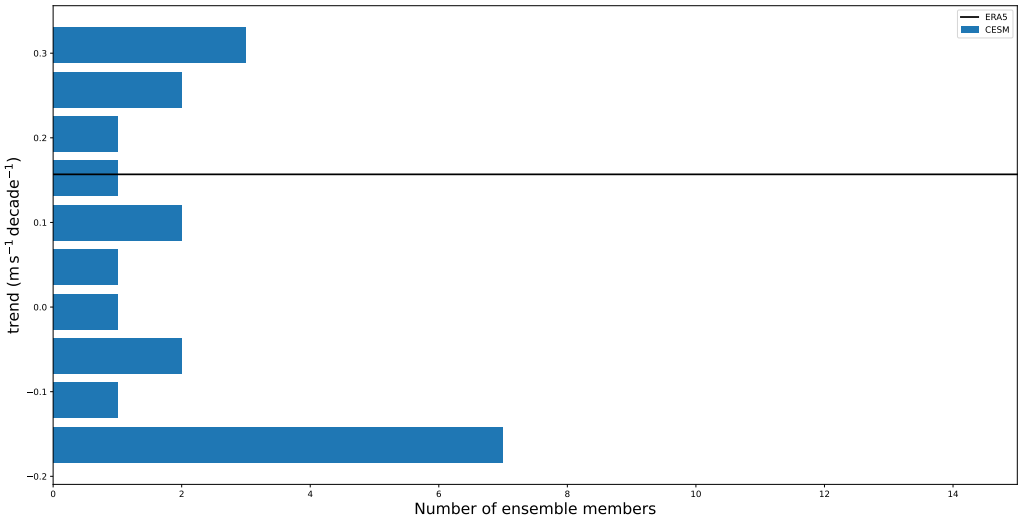

FIG. B2. **Distribution of zonal wind trends in the CESM-LENS:** Histogram of zonal wind speed trends at 250 hPa for the period 1980-2022 averaged between 80°W – 15°W and 30°N – 50°N for the considered CESM-LENS simulations (blue bars) and ERA5 (black line).

Blackport, R., and J. C. Fyfe, 2022: Climate models fail to capture strengthening wintertime North Atlantic jet and impacts on Europe. *Science Advances*, **8**, https://doi.org/10.1126/sciadv.abn3112.

Bogenschutz, P. A., A. Gettelman, H. Morrison, V. E. Larson, C. Craig, and D. P. Schanen, 2018: The path to CAM6: coupled simulations with CAM5.4 and CAM5.5. *Geoscientific Model Development*, **11**, 235–255, https://doi.org/10.5194/gmd-11-235-2018.

Bracegirdle, T. J., H. Lu, R. Eade, and T. Woollings, 2018: Do CMIP5 models reproduce observed low-frequency North Atlantic jet variability? *Geophysical Research Letters*, **45**, 7204–7212, https://doi.org/10.1029/2018GL078965.

Brayshaw, D. J., B. Hoskins, and M. Blackburn, 2009: The Community Earth System Model Version 2 (CESM2). *Journal of Advances in Modeling Earth Systems*, **66**, 2539–2558, https://doi.org/10.1175/2009JAS3078.1.

Brayshaw, D. J., B. Hoskins, and M. Blackburn, 2011: The basic ingredients of the North Atlantic storm track. Part II: Sea surface temperatures. *Journal of the Atmospheric Sciences*, **68**,

1784–1805, https://doi.org/10.1175/2011JAS3674.1.

Browning, K. A., M. E. Hardman, T. W. Harrold, and C. W. Pardoe, 1973: The structure of rainbands within a mid-latitude depression. *Quarterly Journal of the Royal Meteorological Society*, **99**, 215–231, https://doi.org/10.1002/qj.49709942002.

Charney, J. G., 1947: The dynamics of long waves in a baroclinic westerly current. *Journal of the Atmospheric Sciences*, **4**, 136–162, https://doi.org/10.1175/1520-0469(1947)004<0136:TDOLWI>2.0.CO;2.

Danabasoglu, G., and Coauthors, 2020: The Community Earth System Model Version 2 (CESM2). *Journal of Advances in Modeling Earth Systems*, **12**, e2019MS001 916, https://doi.org/10.1002/qj.2378.

Doms, G., and Coauthors, 2011: A description of the non-hydrostatic regional COSMO model. part II: Physical pa- rameterization. Tech. rep., Deutscher Wetterdienst, Offenbach, Germany. https://doi.org/10.5676/DWD_pub/nwv/cosmo-doc_6.00_II,2011.

Drouard, M., G. Rivière, and P. Arbogast, 2013: The north atlantic oscillation response to large-scale atmospheric anomalies in the northeastern pacific. *Journal of the Atmospheric Sciences*, **70 (9)**, 2854–2874, https://doi.org/10.1175/jas-d-12-0351.1.

Drouard, M., G. Rivière, and P. Arbogast, 2015: The link between the North Pacific climate variability and the north atlantic oscillation via downstream propagation of synoptic waves. *Journal of Climate*, **28**, 3957–3976, https://doi.org/10.1175/JCLI-D-14-00552.1.

Eady, E. T., 1949: The dynamics of long waves in a baroclinic westerly current. *Tellus*, **1**, 33–52, https://doi.org/10.1175/1520-0469(1947)004<0136:TDOLWI>2.0.CO;2.

Eichler, T., and W. Higgins, 2006: Climatology and ENSO-related variability of North American extratropical cyclone activity. *Journal of Climate*, **19**, 2076–2093, https://doi.org/10.1175/JCLI3725.1.

Grams, C. M., and Coauthors, 2011: The key role of diabatic processes in modifying the upper-tropospheric wave guide: a North Atlantic case-study. *Quarterly Journal of the Royal Meteorological Society*, **137**, 2174–2193, https://doi.org/10.1002/qj.891.

Green, J. S. A., 1960: A problem in baroclinic stability. *Quarterly Journal of the Royal Meteorological Society*, **86**, 237–251, https://doi.org/10.1002/qj.49708636813.

Guo, R., C. Deser, and L. Terray, 2019: Human influence on winter precipitation trends (1921–2015) over North America and Eurasia revealed by dynamical adjustment. *Geophysical Research Letters*, **46**, 3426–3434, https://doi.org/10.1029/2018GL081316.

Haarsma, R. J., and Coauthors, 2016: High resolution model intercomparison project (HighResMIP v1.0) for CMIP6. *Geoscientific Model Development*, **9**, 4185–4208, https://doi.org/10.5194/gmd-9-4185-2016.

Harrold, T. W., 1973: Mechanisms influencing the distribution of precipitation within baroclinic disturbances. *Quarterly Journal of the Royal Meteorological Society*, **99**, 232–251, https://doi.org/10.1002/qj.49709942003.

Hartmann, D. L., 2007: The atmospheric general circulation and its variability. *Journal of the Meteorological Society of Japan. Ser. II*, **85B**, 123–143, https://doi.org/10.2151/jmsj.85B.123.

Harvey, B., J. Methven, C. Sanchez, and A. Schaefler, 2020: Diabatic generation of negative potential vorticity and its impact on the North Atlantic jet stream. *Quarterly Journal of the Royal Meteorological Society*, **146**, 1477—-1497, https://doi.org/10.1002/qj.3747.

Heinze-Deml, C., S. Sippel, A. G. Pendergrass, F. Lehner, and N. Meinshausen, 2021: Latent Linear Adjustment Autoencoder v1.0: a novel method for estimating and emulating dynamic precipitation at high resolution. *Geoscinetific Model Development*, **14**, 4977–4999, https://doi.org/10.5194/gmd-14-4977-2021.

Held, I. M., 1993: Large-scale dynamics and global warming. *Bulletin of the American Meteorological Society*, **74 (2)**, 228–242, https://doi.org/10.1175/1520-0477(1993)074<0228:LSDAGW>2.0.CO;2.

Held, I. M., and B. J. Soden, 2006: Robust responses of the hydrological cycle to global warming. *Journal of Climate*, **19**, 5686–5699, https://doi.org/10.1175/JCLI3990.1.

Hersbach, H., and Coauthors, 2020: The ERA5 global reanalysis. *Quarterly Journal of the Royal Meteorological Society*, **146**, 1999–2049, https://doi.org/10.1002/qj.3803.

Hersbach, H., and Coauthors, 2023: ERA5 hourly data on single levels from 1940 to present. Copernicus Climate Change Service (C3S) Climate Data Store (CDS), dataset, https://doi.org/10.24381/cds.adbb2d47.

Hogan, R. J., and A. Bozzo, 2018: A flexible and efficient radiation scheme for the ECMWF model. *Journal of Advances in Modeling Earth Systems*, **10**, 1990–2008, https://doi.org/10.1029/2018MS001364.

Hoskins, B. J., I. James, and G. White, 1983: The shape, propagation and mean-flow interaction of large-scale weather systems. *Journal of the Atmospheric Sciences*, **40**, 1595–1612, https://doi.org/10.1175/1520-0469(1983)040,1595:TSPAMF.2.0.CO;2.

Hoskins, B. J., and D. J. Karoly, 1981: The steady linear response of a spherical atmosphere to thermal and orographic forcing. *Journal of the Atmospheric Sciences*, **38**, 1179–1196, https://doi.org/10.1175/1520-0469(1981)038<1179:TSLROA>2.0.CO;2.

Hoskins, B. J., and P. J. Valdes, 1990a: On the existence of storm-tracks. *Journal of the Atmospheric Sciences*, **47**, 1854–1864, https://doi.org/10.1175/1520-0469(1990)047<1854:OTEOST>2.0.CO;2.

Hoskins, B. J., and P. J. Valdes, 1990b: On the existence of storm-tracks. *Journal of Atmospheric Sciences*, **47 (15)**, 1854–1864, https://doi.org/10.1175/1520-0469(1990)047<1854:OTEOST>2.0.CO;2.

Hotta, D., and H. Nakamura, 2011: On the significance of the sensible heat supply from the ocean in the maintenance of the mean baroclinicity along storm tracks. *Journal of Climate*, **24**, 3377–3401, https://doi.org/10.1175/2010JCLI3910.1.

Hunke, E., W. Lipscomb, A. Turner, and S. Jeffery, N. ans Elliott, 2015: ICE: The Los Alamos Sea Ice Model documentation and software user's manual version 5.1 LA-CC-06-012. Tech. rep., Los Alamos National Laboratory, Santa Fe, NM, USA.

Igel, A. L., and S. C. van der Heever, 2014: The role of latent heating in warm frontogenesis. *Quarterly Journal of the Royal Meteorological Society*, **140**, 139–150, https://doi.org/10.1002/qj.2118.

Jablonowski, C., and D. L. Williamson, 2006: A baroclinic instability test case for atmospheric model dynamical cores. *Quarterly Journal of the Royal Meteorological Society*, **132**, 2943–2975, https://doi.org/10.1256/qj.06.12.

Kidston, J., A. A. Scaife, S. C. Hardiman, D. M. Mitchell, N. Butchart, B. M. P., and L. J. Gray, 2015: Stratospheric influence on tropospheric jet streams, storm tracks and surface weather. *Nature Goescience*, **8**, 433–440, https://doi.org/10.1038/ngeo2424.

Kuwano-Yoshida, A., S. Minobe, and S.-P. Xie, 2010: Precipitation response to the Gulf Stream in an atmospheric GCM. *Journal of Climate*, **23**, 3676–3698, https://doi.org/10.1175/2010jcli3261.1.

Lawrence, D., and Coauthors, 2019: The Community Land Model version 5: Description of new features, benchmarking, and impact of forcing uncertainty. *Journal of Advances in Modeling Earth Systems*, **11**, 4245–4287, https://doi.org/10.1029/2018MS001583.

Lee, J.-Y., and Coauthors, 2021: Future global climate: Scenario-based projections and near-term information. *Climate Change 2021: The Physical Science Basis. Contribution of Working Group I to the Sixth Assessment Report of the Intergovernmental Panel on Climate Change*, V. Masson-Delmotte, P. Zhai, A. Pirani, S. Connors, C. Péan, S. Berger, N. Caud, Y. Chen, L. Goldfarb, M. Gomis, M. Huang, K. Leitzell, E. Lonnoy, J. Matthews, T. Maycock, T. Waterfield, O. Yelekçi, R. Yu, and B. Zhou, Eds., Cambridge University Press, Cambridge, United Kingdom and New York, NY, USA, chap. 4, 553–672.

Lee, S., and H. kyung Kim, 2003: The dynamical relationship between subtropical and eddy-driven jets. *Journal of the Atmospheric Sciences*, **60 (12)**, 1490–1503, https://doi.org/10.1175/1520-0469(2003)060<1490:tdrbsa>2.0.co;2.

Lehner, F., C. Deser, and L. Terray, 2017: Toward a new estimate of "time of emergence" of anthropogenic warming: Insights from dynamical adjustment and a large initial-condition model ensemble. *Journal of Climate*, **30**, 7739–7756, https://doi.org/10.1175/JCLI-D-16-0792.1.

Li, C., and J. J. Wettstein, 2012: Thermally driven and eddy-driven jet variability in reanalysis. *Journal of Climate*, **25 (5)**, 1587–1596, https://doi.org/10.1175/jcli-d-11-00145.1.

Li, H., M. S. Wigmosta, H. Wu, M. Huang, Y. Ke, A. M. Coleman, and L. R. Leung, 2013: A physically based runoff routing model for land surface and Earth system models. *Journal of Hydrometeorology*, **14**, 808–828, https://doi.org/10.1175/JHM-D-12-015.1.

Lindzen, R. S., and B. Farrell, 1980: A simple approximate result for the maximum growth rate of baroclinic instabilities. *Journal of the Atmospheric Sciences*, **37**, 1648–1654, https://doi.org/10.1175/1520-0469(1980)037<1648:ASARFT>2.0.CO;2.

Lorenz, D. J., and E. T. DeWeaver, 2007: Tropopause height and zonal wind response to global warming in the IPCC scenario integrations. *Journal of Geophysical Research: Atmospheres*, **112 (D10)**, https://doi.org/https://doi.org/10.1029/2006JD008087.

Lorenz, D. J., and D. L. Hartmann, 2003: Eddy–zonal flow feedback in the Northern Hemisphere winter. *Journal of climate*, **16 (8)**, 1212–1227, https://doi.org/10.1175/1520-0442(2003)16<1212:EFFITN>2.0.CO;2.

Maher, P., M. E. Kelleher, P. G. Sansom, and J. Methven, 2020: Is the subtropical jet shifting poleward? *Climate Dynamics*, **54**, 1741–1759, https://doi.org/10.1007/s00382-019-05084-6.

Manney, G. L., and M. I. Hegglin, 2018: Seasonal and regional variations of long-term changes in upper-tropospheric jets from reanalyses. *Journal of Climate*, **31**, 423–448, https://doi.org/10.1175/JCLI-D-17-0303.1.

Martin, J. E., 2021: Recent trends in the waviness of the Northern Hemisphere wintertime polar and subtropical jets. *Journal of Geophysical Research: Atmospheres*, **126**, e2020JD033 668, https://doi.org/10.1029/2020JD033668.

Minobe, S., A. Kuwano-Yoshida, N. Komori, S.-P. Xie, and R. J. Small, 2008: Influence of the Gulf Stream on the troposphere. *Nature*, **452**, https://doi.org/10.1038/nature06690.

Nakamura, H., 1992: Midwinter suppression of baroclinic wave activity in the Pacific. *Journal of the Atmospheric Sciences*, **49**, 1629–1642, https://doi.org/10.1175/1520-0469(1992)049<1629:MSOBWA>2.0.CO;2.

Neale, R. B., and B. J. Hoskins, 2001: A standard test for AGCMs including their physical parametrizations: I: The proposal. *Atmospheric Science Letters*, **101**, 101–107, https://doi.org/10.1256/qj.06.12.

Novak, L., M. H. P. Ambaum, and R. Tailleux, 2015: The life cycle of the North Atlantic storm track. *Journal of the Atmospheric Sciences*, **72**, 821–833, https://doi.org/10.1175/JAS-D-14-0082.1.

O'Neill, B. C., and Coauthors, 2016: The scenario model intercomparison project (ScenarioMIP) for CMIP6. *Geoscientific Model Development*, **9**, 3461–3482, https://doi.org/10.5194/gmd-9-3461-2016.

O'Reilly, H., S. Minobe, A. Kuwano-Yoshida, and T. Woollings, 2017: The Gulf Stream influence on wintertime North Atlantic jet variability. *Quarterly Journal of the Royal Meteorological Society*, **143**, 173–183, https://doi.org/10.1002/qj.2907.

Orlanski, I., 1998: Poleward deflection of storm tracks. *Journal of the Atmospheric Sciences*, **55 (16)**, 2577–2602.

Orr, A., P. Bechtold, J. Scinocca, M. Ern, and M. Janiskova, 2010: Improved middle atmosphere climate and forecasts in the ECMWF model through a nonorographic gravity wave drag parameterization. *Journal of Climate*, **23**, 5905–5926, https://doi.org/10.1175/2010JCLI3490.1,2010.

Owen, L. E., J. L. Catto, D. B. Stephenson, and N. J. Dunstone, 2021: Compound precipitation and wind extremes over Europe and their relationship to extratropical cyclones. *Weather and Climate Extremes*, **33**, 100 342, https://doi.org/10.1016/j.wace.2021.100342.

Papritz, L., and T. Spengler, 2015: Analysis of the slope of isentropic surfaces and its tendencies over the north atlantic. *Quarterly Journal of the Royal Meteorological Society*, **141 (693)**, 3226–3238.

Parfitt, R., and A. Czaja, 2016: On the contribution of synoptic transients to the mean atmospheric state in the gulf stream region. *Quarterly Journal of the Royal Meteorological Society*, **142 (696)**, 1554–1561, https://doi.org/10.1002/qj.2689.

Parfitt, R., A. Czaja, and Y.-O. Kwon, 2017: The impact of SST resolution change in the ERA-interim reanalysis on wintertime Gulf Stream frontal air-sea interaction. *Geophysical Research Letters*, **44 (7)**, 3246–3254, https://doi.org/10.1002/2017GL073028.

Peings, Y., J. Cattieux, S. J. Vavrus, and G. Magnusdottir, 2018: Projected squeezing of the wintertime North-Atlantic jet. *Environmental Research Letters*, **13**, 074 016, https://doi.org/10.1088/1748-9326/aacc79.

Peng, S., and J. S. Whitaker, 1999: Mechanisms determining the atmospheric response to midlatitude SST anomalies. *Journal of Climate*, **12**, 1393–1408, https://doi.org/10.1175/1520-0442(1999)012<1393:MDTART>2.0.CO;2.

Pfahl, S., and H. Wernli, 2012: Quantifying the relevance of cyclones for precipitation extremes. *Journal of Climate*, **25 (19)**, 1288–1297, https://doi.org/10.1002/qj.829.

Pomroy, H. R., and A. J. Thorpe, 2000: The evolution and dynamical role of reduced upper-tropospheric potential vorticity in intensive observing period one of FASTEX. *Monthly weather review*, **128**, 1817–1834, https://doi.org/10.1175/1520-0493(2000)128<1817:TEADRO>2.0.CO;2.

Priestley, M. D. K., and J. L. Catto, 2022: Future changes in the extratropical storm tracks and cyclone intensity, wind speed, and structure. *Weather and Climate Dynamics*, **3**, 337–360, https://doi.org/10.5194/wcd-3-337-2022.

Rivière, G., 2009: Effect of latitudinal variations in low-level baroclinicity on eddy life cycles and upper-tropospheric wave-breaking processes. *Journal of the Atmospheric Sciences*, **66**, 1569–1592.

Rivière, G., M. Wimmer, P. Arbogast, J.-M. Piriou, J. Delanoë, C. Labadie, Q. Cazenave, and J. Pelon, 2021: The impact of deep convection representation in a global atmospheric model on the warm conveyor belt and jet stream during NAWDEX IOP6. *Weather and Climate Dynamics*, **2**, 1011–1031, https://doi.org/10.5194/wcd-2-1011-2021.

Rodgers, S.-S., K. B. Lee, and Coauthors, 2021: Ubiquity of human-induced changes in climate variability. *Earth System Dynamics*, **12**, 1393–1411, https://doi.org/10.5194/esd-12-1393-2021.

Sampe, T., H. Nakamura, A. Goto, and W. Ohfuchi, 2010: Significance of a midlatitude SST frontal zone in the formation of a storm track and an eddy-driven westerly jet. *Journal of Climate*, **23**, 1793–1814, https://doi.org/10.1175/2009JCLI3163.1.

Schemm, S., 2023: Toward eliminating the decades-old "too zonal and too equatorward" storm-track bias in climate models. *Journal of Advances in Modeling Earth Systems*, **15 (2)**, e2022MS003 482, https://doi.org/https://doi.org/10.1029/2022MS003482.

Schemm, S., L. Papritz, and G. Rivière, 2022: Storm track response to uniform global warming downstream of an idealized sea surface temperature front. *Weather and Climate Dynamics*, https://doi.org/10.5194/wcd-3-601-2022.

Schemm, S., and G. Rivière, 2019: On the efficiency of baroclinic eddy growth and how it reduces the North Pacific storm-track intensity in midwinter. *Journal of Climate*, **32**, 8373–8398, https://doi.org/10.1175/JCLI-D-19-0115.1.

Schemm, S., G. Rivière, L. M. Ciasto, and C. Li, 2018: Extratropical cyclogenesis changes in connection with tropospheric ENSO teleconnections to the North Atlantic: Role of stationary and transient waves. *Journal of the Atmospheric Sciences*, **17**, 3943–3964, https://doi.org/10.1175/JAS-D-17-0340.1.

Schemm, S., H. Wernli, and H. Binder, 2021: The storm-track suppression over the western North Pacific from a cyclone life-cycle perspective. *Weather and Climate Dynamics*, **2**, 55–69, https://doi.org/10.5194/wcd-2-55-2021.

Schemm, S., H. Wernli, and L. Papritz, 2013: Warm conveyor belts in idealized moist baroclinic wave simulations. *Journal of the Atmospheric Sciences*, **70**, 627–652, https://doi.org/10.1175/JAS-D-12-0147.1.

Screen, J. A., and I. Simmonds, 2010: The central role of diminishing sea ice in recent Arctic temperature amplification. *Nature*, **464 (7293)**, 1334–1337, https://doi.org/10.1038/nature09051.

Shaw, T., and Coauthors, 2016: Storm track processes and the opposing influences of climate change. *Nature Geoscience*, **9 (9)**, 656–664.

Sheldon, L., A. Czaja, B. Vanniére, C. Morcrette, B. Sohet, M. Casado, and D. Smith, 2017: A 'warm path' for Gulf Stream–troposphere interactions. *Tellus A: Dynamic Meteorology and Oceanography*, **69**, 1299 397, https://doi.org/10.1080/16000870.2017.1299397.

Simmons, A. J., 2022: Trends in the tropospheric general circulation from 1979 to 2022. *Weather and Climate Dynamics*, **3 (3)**, 777–809, https://doi.org/10.5194/wcd-3-777-2022.

Simpson, I. R., T. A. Shaw, and R. Seager, 2014: A diagnosis of the seasonally and longitudinally varying midlatitude circulation response to global warming. *Journal of the Atmospheric Sciences*, **71**, 2489—-2515, https://doi.org/10.1175/JAS-D-13-0325.1.

Sippel, S., N. Meinshausen, A. Merrifield, F. Lehner, A. G. Pendergrass, E. Fischer, and R. Knutti, 2019: Human influence on winter precipitation trends (1921–2015) over North America and Eurasia revealed by dynamical adjustment. *Journal of Climate*, **32**, 5677–5699, https://doi.org/10.1175/JCLI-D-18-0882.1.

Small, R. J., R. A. Tomas, and F. O. Bryan, 2014: Storm track response to ocean fronts in a global high-resolution climate model. *Climate dynamics*, **43**, 805–828, https://doi.org/10.1007/s00382-013-1980-9.

Smoliak, B. V., J. M. Wallace, P. Lin, and Q. Fu, 2015: Dynamical adjustment of the Northern Hemisphere surface air temperature field: Methodology and application to observations. *Journal of Climate*, **28**, 1613–1629, https://doi.org/10.1175/JCLI-D-14-00111.1.

Stoelinga, M. T., 1996: A potential vorticity-based study of the role of diabatic heating and friction in a numerically simulated baroclinic cyclone. *Monthly weather review*, **124**, 849–874, https://doi.org/10.1175/1520-0493(1996)124<0849:APVBSO>2.0.CO;2.

Thompson, D. W. J., and T. Birner, 2012: On the linkages between the tropospheric isentropic slope and eddy fluxes of heat during northern hemisphere winter. *Journal of the Atmospheric Sciences*, **69**, 1811–1823, https://doi.org/10.1175/JAS-D-11-0187.1.

Tiedke, M., 1989: A comprehensive mass flux scheme for cumulus parameterization in large-scale models. *Monthly Weather Review*, **117**, 1779–1800, https://doi.org/10.1175/1520-0493(1989)117<1779:ACMFSF>2.0.CO;2.

Vallis, G. K., 2017: *Atmospheric and Oceanic Fluid Dynamics: Fundamentals and Large-Scale Circulation*. 2nd ed., Cambridge University Press, https://doi.org/10.1017/9781107588417.

Van Delden, A., 1999: The slope of isentropes constituting a frontal zone. *Tellus A: Dynamic Meteorology and Oceanography*, **51**, 603–611, https://doi.org/10.3402/tellusa.v51i5.14479.

Wallace, C., and M. Joshi, 2018: Comparison of land–ocean warming ratios in updated observed records and CMIP5 climate models. *Environmental Research Letters*, **13**, 114 011, https://doi.org/10.1088/1748-9326/aae46f.

Weijenborg, C., and T. Spengler, 2020: Diabatic heating as a pathway for cyclone clustering encompassing the extreme storm Dagmar. *Geophysical Research Letters*, **47**, e2019GL085 777, https://doi.org/10.1029/2019GL085777.

Wernli, H., and H. C. Davies, 1997: A lagrangian-based analysis of extratropical cyclones. I: The method and some applications. *Quarterly Journal of the Royal Meteorological Society*, **123**, 467–489, https://doi.org/10.1002/qj.49712353811.

Wilks, D. S., 2016: The stippling shows statistically significant grid points. *Bulletin of the American Meteorological Society*, **97**, 2263–2273, https://doi.org/10.1175/BAMS-D-15-00267.1.

Wimmer, M., G. Rivière, P. Arbogast, J.-M. Piriou, J. Delanoë, C. Labadie, Q. Cazenave, and J. Pelon, 2022: Diabatic processes modulating the vertical structure of the jet stream above the cold front of an extratropical cyclone: sensitivity to deep convection schemes. *Weather and Climate Dynamics*, **3**, 863–882, https://doi.org/10.5194/wcd-3-863-2022.

Woollings, T., 2010: Dynamical influences on european climate: an uncertain future. *Philosophical Transactions of the Royal Society A: Mathematical, Physical and Engineering Sciences*, **368 (1924)**, 3733–3756, https://doi.org/10.1098/rsta.2010.0040.

Woollings, T., M. Drouard, D. M. H. O'Reilly, C. H. Sexton, and C. McSweeney, 2023: Trends in the atmospheric jet streams are emerging in observations and could be linked to tropical warming. *Communications Earth and Environment*, **4**, 1–8, https://doi.org/10.1038/s43247-023-00792-8.

Woollings, T., J. M. Gregory, J. G. Pinto, M. Reyers, and D. J. Brayshaw, 2012: Response of the North Atlantic storm track to climate change shaped by ocean–atmosphere coupling. *Nature Geoscience*, **5 (5)**, 313–317.

Woollings, T., L. Papritz, C. Mbengue, and T. Spengler, 2016: Diabatic heating and jet stream shifts: A case study of the 2010 negative North Atlantic Oscillation winter. *Geophysical Research Letters*, **43**, 9994–10 002, https://doi.org/10.1002/2016GL070146.

Yadav, P., and D. M. Straus, 2017: Circulation response to fast and slow MJO episodes. *Monthly Weather Review*, **145**, 1577–1596, https://doi.org/10.1175/MWR-D-16-0352.1.

Yu, B., and H. Lin, 2016: Tropical atmospheric forcing of the wintertime North Atlantic Oscillation. *Journal of Cliamte*, **29**, 1755–1772, https://doi.org/10.1175/JCLI-D-15-0583.1.

Yuval, J., and Y. Kaspi, 2016: Eddy activity sensitivity to changes in the vertical structure of baroclinicity. *Journal of the Atmospheric Sciences*, **73**, 1709–1726, https://doi.org/10.1175/JAS-D-15-0128.1.

Zängl, G., D. Reinert, P. Rípodas, and M. Baldauf, 2015: The ICON (ICOsahedral Non-hydrostatic) modelling framework of DWD and MPI-M: Description of the non-hydrostatic dynamical core. *Journal of the Atmospheric Sciences*, **141**, 563–579, https://doi.org/10.1002/qj.2378.